ANL-ET-04/24

Calculation of Tin Atomic Data and Plasma Properties

prepared by
Energy Technology Division
Argonne National Laboratory

Argonne National Laboratory is managed by
The University of Chicago for the U. S. Department of Energy

About Argonne National Laboratory

Argonne is managed by The University of Chicago for the U.S. Department of Energy under contract W-31-109-Eng-38. The Laboratory's main facility is outside Chicago, at 9700 South Cass Avenue, Argonne, Illinois 60439. For information about Argonne and its pioneering science and technology programs, see www.anl.gov.

Availability of This Report

This report is available, at no cost, at http://www.osti.gov/bridge. It is also available on paper to U.S. Department of Energy and its contractors, for a processing fee, from:

U.S. Department of Energy
Office of Scientific and Technical Information
P.O. Box 62
Oak Ridge, TN 37831-0062
phone (865) 576-8401
fax (865) 576-5728
reports@adonis.osti.gov

ANL-ET-04/24

Calculation of Tin Atomic Data and Plasma Properties

by
V. Morozov, V. Tolkach, and A. Hassanein
Energy Technology Division, Argonne National Laboratory

September 2004

Argonne National Laboratory is managed by
The University of Chicago for the U. S. Department of Energy

CONTENTS

ABSTRACT....1
INTRODUCTION....1
1. HFS ENERGY LEVELS AND OTHER DATA....2
2. ION STATES AND POPULATIONS OF ATOMIC LEVELS....4
3. THERMODYNAMIC PLASMA PROPERTIES AND EQUATION OF STATE....7
4. DETAILED SET OPACITIES IN WIDE ENERGY RANGE....8
5. PLANCK GROUP AVERAGED OPACTITES IN WIDE ENERGY RANGE....9
6. HF ENERGY LEVELS AND OTHER DATA FOR EUV EMITTING TIN ION SPECIES...11
7. DETAILED TIN EUV TRANSITIONS....17
8. DETAILED TIN EUV OPACITIES....22
CONCLUSION....23
ACKNOWLEDGMENTS....24
REFERENCES....24
APPENDIX A....26
APPENDIX B....29
APPENDIX C....31

FIGURES

Fig. 1: Concentrations of tin ions for various densities 5
Fig. 2: Calculations from equation of state for tin ions at various densities.....7
Fig. 3: Optical coefficients for tin plasma at T = 26 eV and N = 10^{16} cm^{-3} 10
Fig. 4: Planck mean optical coefficients for tin plasma.....10
Fig. 5: Experimental data vs. calculation for Sn VIII $4d^7 - 4d^6 5p^1$ transition.....19
Fig. 6: Calculation of tin EUV transitions by the HEIGHTS-ATOM code.....20
Fig. 7: Calculation of tin EUV transitions by the Cowan code 21
Fig. 8: Tin plasma optical coefficients in the EUV range.....23

TABLES

Table 1: Concentration (in percent) of xenon ions at 10^{17} cm^{-3}.....6
Table 2: Concentration (in percent) of tin ions at 10^{17} cm^{-3} 6
Table 3: Energies of Xe XI inner shells by *LSD* HF and average term HF.....13
Table 4: Energies of Sn VIII inner shells by *LSD* HF and average term HF.....13
Table 5: O I $2p^3$ 3s excited state energy levels.....14
Table 6: Ar II $3p^4$ 3d excited state energy levels.....14
Table 7: Sn VIII $4d^7$ ground state energy levels.....15
Table 8: Xe XI $4d^8$ ground state energy levels (in cm^{-1}) 16
Table 9: Xe XI $4d^7$ 5p excited state energy levels (in cm^{-1}) 16
Table 10: Summary of the tin EUV transitions 22

ABSTRACT

This report reviews the major methods and techniques we use in generating basic atomic and plasma properties relevant to extreme ultraviolet (EUV) lithography applications. The basis of the work is the calculation of the atomic energy levels, transitions probabilities, and other atomic data by various methods, which differ in accuracy, completeness, and complication. Later on, we calculate the populations of atomic levels and ion states in plasmas by means of the collision-radiation equilibrium (CRE) model. The results of the CRE model are used as input to the thermodynamic functions, such as pressure and temperature from the internal energy and density (equation of state), electric resistance, thermal conduction, and other plasma properties. In addition, optical coefficients, such as emission and absorption coefficients, are generated to resolve a radiation transport equation (RTE). The capabilities of our approach are demonstrated by generating the required atomic and plasma properties for tin ions and plasma within the EUV region near 13.5 nm.

INTRODUCTION

To meet the requirements of the Intel Lithography Roadmap goals for high volume manufacturing in the future [1] and International SEMATECH's EUV Source Program goals [2], the EUV source is required to have a power of 80-120 W at 13.5 nm (2% bandwidth). Various laser produced plasma (LPP) and gas discharge produced plasma (DPP) devices are under development and investigation by different research groups. Both types of EUV sources have advantages and disadvantages. At present, none of the current EUV sources can deliver enough power levels demanded by commercial chip manufacturers.

The efficiency of generating EUV radiation is the key factor in successful development of the source. The leading EUV groups are using a variety of scientific and engineering approaches to maximize EUV brightness from their devices. A common technique is the increase of the optimized overall conversion efficiency of a device, because it minimizes the required input power for a required EUV output. Because many physical processes are involved, and many technical problems need to be solved, when optimizing a particular EUV device, only computer modeling can generate a complete picture at a reasonable pace.

We are developing an integrated model to simulate the environment of the EUV source and optimize the output of the source. The model describes the hydrodynamic and optical processes that occur in EUV devices. It takes into account plasma evolution and magneto-hydrodynamic (MHD) processes as well as photon radiation transport. It uses the total variation diminishing scheme in the Lax-Friedrich formulation for the description of magnetic compression and diffusion in a cylindrical geometry. Also under development are models for opacity calculations: a collisional radiation equilibrium model, a self-consistent field model with Auger processes, and a nonstationary kinetic model. Radiation transport for both continuum and lines with detailed spectral profiles is taken into account. The developed models are being integrated into the HEIGHTS-EUV computer simulation package [3, 4]. Being self-consistent,

the HEIGHTS-EUV package can generate all required information and is completely independent of the data from other external packages. Furthermore, experimentally (or numerically) obtained reliable data can be incorporated into HEIGHTS-EUV to increase the overall accuracy and efficiency of the simulation results.

The focus of this report is the major methods and techniques we use in our HEIGHTS-ATOM code to generate basic atomic and plasma properties. Based upon accurately generated atomic energy levels, transition probabilities, and other atomic data, we can calculate the populations of atomic levels and ion states in plasma by means of the CRE model. In turn, the results of the CRE model are used as input to thermodynamic functions, such as those for pressure and temperature from the internal energy and density (equation of state), electric resistance, thermal conduction, and other plasma properties. Optical coefficients are also generated to resolve the RTE. Combining the generated properties with an appropriate description of an EUV device in terms of the MHD boundary conditions, we are able to simulate the dynamics of the device and its total radiation output. The accuracy and completeness of atomic data are key factors in the successful numerical simulation of the EUV device.

This report contains the results of our computer simulation of the tin atomic data and plasma properties in tabulated form. The calculation of atomic properties by the Hartree-Fock-Slater (HFS) approximation is described in the first section. Section 2 is devoted to the description of the CRE model, which is used to obtain the populations of the atomic levels and the ion composition of the plasma. The calculation of thermodynamic plasma properties and the equation of state are described in the third section. The resolution of the radiation transport equation in a wide spectral range depends upon the completeness of the optical coefficients, which are discussed in Section 4. The Planck mean opacities are presented in Section 5. The next three sections are primarily dedicated to calculating highly accurate EUV information for tin. Section 6 discusses the limitations of using the simplified methods for generating EUV atomic data and describes the advanced *LS*-dependent Hartree-Fock (*LSD* HF) atomic method. Detailed EUV transitions are presented in Section 7. Finally, Section 8 presents calculations of tin EUV opacities with very high resolution.

1. HFS ENERGY LEVELS AND OTHER DATA

In modeling the dynamics and the output of an EUV source, one needs to distinguish two aspects. First, in solving the hydrodynamic part of the problem, the plasma internal energy must be corrected and re-distributed accordingly to the radiation transport. A key element in this process is the completeness of the radiant energy redistribution in the whole plasma domain within the very broad spectral range of participating photons. The second aspect is the detailed calculation of the effective radiation of the EUV source within the operating energy range of 13.5 ± 2% nm. In this case, the calculation of the radiation transport must be oriented to the accurate accounting of only those photons, whose energies are within the narrow EUV range.

The simulation of the dynamics of the plasma evolution typically involves a wide range of temperature and density values and a very complicated ionic structure. From the atomic physics viewpoint, detailed resolution of each possible level for each possible ion (and

consequently, each electronic transition in the ion) in a wide range of temperatures, densities, and energies is enormously laborious, especially when one is accounting for the fine structure of each split level. The difficulties come from the very large number of atomic terms and split levels. For example, to split a d^5 shell, one needs to account for 16 terms and 37 levels. The f^7 shell will have 119 terms and 327 levels. In approximation of configurations, the transition $4d^n - 4d^{n-1}4f$ will only have one strong line, while splitting the shells into levels replaces this line by several hundred weak lines. Knowing that the total transition strength is unchanged, the radiation in strong lines may be collapsed for a dense plasma, while the radiation in weak lines stays optically transparent. The line splitting may dramatically influence the total hydrodynamic behavior of a plasma through the radiation transport mechanism [5].

The results of theoretical approximations of atomic data strongly depend on the chosen theoretical models [6 - 8], and this is particularly true for intermediate- and high-Z materials. To describe a spherically symmetrical quantum system, the self-consistent field methods, such as Dirac-Fock (DF) or Hartree-Fock (HF) methods, are believed to be the most effective. However, the very large number of ions and their atomic levels and transitions involved into the plasma computation, limits their applicability. In consistently solving the MHD equations and the RTE, the plasma properties, opacities, equation of state, and ion concentrations can be obtained from the structures of atomic levels and transition probabilities, calculated by simplified methods. One such method is the HFS approximation [9], which allows the determination of the energies and other atomic characteristics for each *nl*-configuration of each ion that might exist in the plasma. The simplification of the method normally results in the shift of some spectral lines from their true places by several percent, which is not problematic in determining the integral radiation flux. Nevertheless, we cannot neglect the fine structure of open shells, and have thus combined the HFS methods with the splitting of the energy levels and spectral lines by means of the Racah theory of angular momentum within the framework of perturbation theory [10, 11, 5].

The accuracy of the HFS model is typically within several percents for the split levels. However, this accuracy is not good enough for the second part of our project, which involves determining the EUV output of the source within the very narrow 2% bandwidth. [To obtain a spectroscopic accuracy of the EUV optical coefficients, the atomic data are calculated by the *LS*-dependent (*LSD*) HF method, as discussed in Section 6.]

In the HFS method the potential of direct electron interaction is calculated from the radial wavefunctions of participating electrons, and exchange interactions are averaged in the form of the exchange potential V_{ex}. The radial wavefunction of an atom can be represented as the product of radial wavefunctions $P_{nl}(r)$ of the electrons. It is assumed that all q_{nl} equivalent electrons have the same radial wavefunction:

$$\left(\frac{d^2}{dr^2} + \frac{2Z(r)}{r} + V_{ex}(r) - \frac{l(l+1)}{r^2} + \varepsilon_{nl}\right) P_{nl}(r) = 0,$$

$$\frac{Z(r)}{r} = \int_r^\infty \frac{Z_0 - \int_0^{r_1} \rho(x)dx}{r_1^2} dr_1, \quad V_{ex}(r) = -\frac{3}{2}\left(\frac{3}{\pi}\rho\right)^{\frac{1}{3}}, \quad \rho(r) = \sum_{nl} q_{nl} P_{nl}^2(r). \tag{1.1}$$

Traditionally, in atomic physics, the energies are expressed in Ry, and distances are in a_0 or Bohr units. In the above equations, ε_{nl} is binding energy of the electron, $Z(r)$ is the effective charge of the ion field, Z_0 is the nuclear charge, and $\rho(r)$ is the electron density.

From solution of the HFS equations, one may find one radial wavefunction for each shell of the atom or ion. We normally calculate the functions for each ion, starting from the neutral and ending with the totally ionized core. Obtained wavefunctions are used to later calculate relativistic corrections, transition wavelengths, and dipole transitions from the ground state to the highly excited state (principal quantum number may reach up to 10), allowed by the selection rules. Discrete transitions from inner shells with energies limited to the value dependent on ionization potential were also taken into account. Photoionization crosssections were calculated for all inner and excited states. Detailed spin-orbit splitting of non-filled shells was implemented outside the HFS, but within the CRE model, by using Slater integrals F^k, G^k, and constants of spin-orbit splitting ξ^k as described in Ref. 5.

2. ION STATES AND POPULATIONS OF ATOMIC LEVELS

To describe the populations of atomic levels, we utilize the CRE model, which is equally applicable for low, medium, and high temperature ranges. The CRE model accounts for the excitation and ionization processes that can take place in a plasma. The fact that the CRE model considers the transitions between all atomic levels is of particular importance. Nonlocal effects are accounted for in the form of an escape factor [12, 13], which neglects by photoexcitation in continuum and reduces the strength of spontaneous transitions. Such an approximation fairly describes the plasma behavior in the condition of absence of an external source of hard radiation.

The plasma ionization state and population levels n_i for a prescribed set of temperatures and densities are calculated according to the system of kinetic equations in stationary form:

$$\frac{dn_i}{dt} = -n_i \sum_{j \neq i} K_{ij} + \sum_{i \neq j} n_j K_{ji} = 0. \qquad \textbf{(2.1)}$$

The population of atomic level *i* is determined by the set of transitions from this level to other levels *j* with transition rates K_{ij}, as well as transitions from other levels *j* to this level *i* with transition rates K_{ji}. One equation is written for each atomic level. If level *i* defines the ground state, then the population of this atomic level gives the concentration of the ion in the plasma. Impact-electron excitation and de-excitation, impact electron ionization, three-body recombination, spontaneous transition, and photo- and di-electronic recombination are included in calculation of total rates of electron transition. From the known population of levels, ion and electron concentrations N_i and N_e are defined for a given temperature.

A numerical simulation of concentration of tin ions calculated by the CRE model with splitting HFS atomic levels is presented in Fig. 1 for various plasma densities. Due to ionization of the *d*-shell, the ions change very quickly when temperature increases. This condition results in a low concentration of the major ion, hardly larger than 50% at best. At the same time, the clear advantage of tin as an EUV working element is that several ions are EUV productive,

which noticeably widen the range of the required temperature in the device. This situation is especially true at low density, when EUV emitting ions are appearing at slightly higher temperature and not changing as fast.

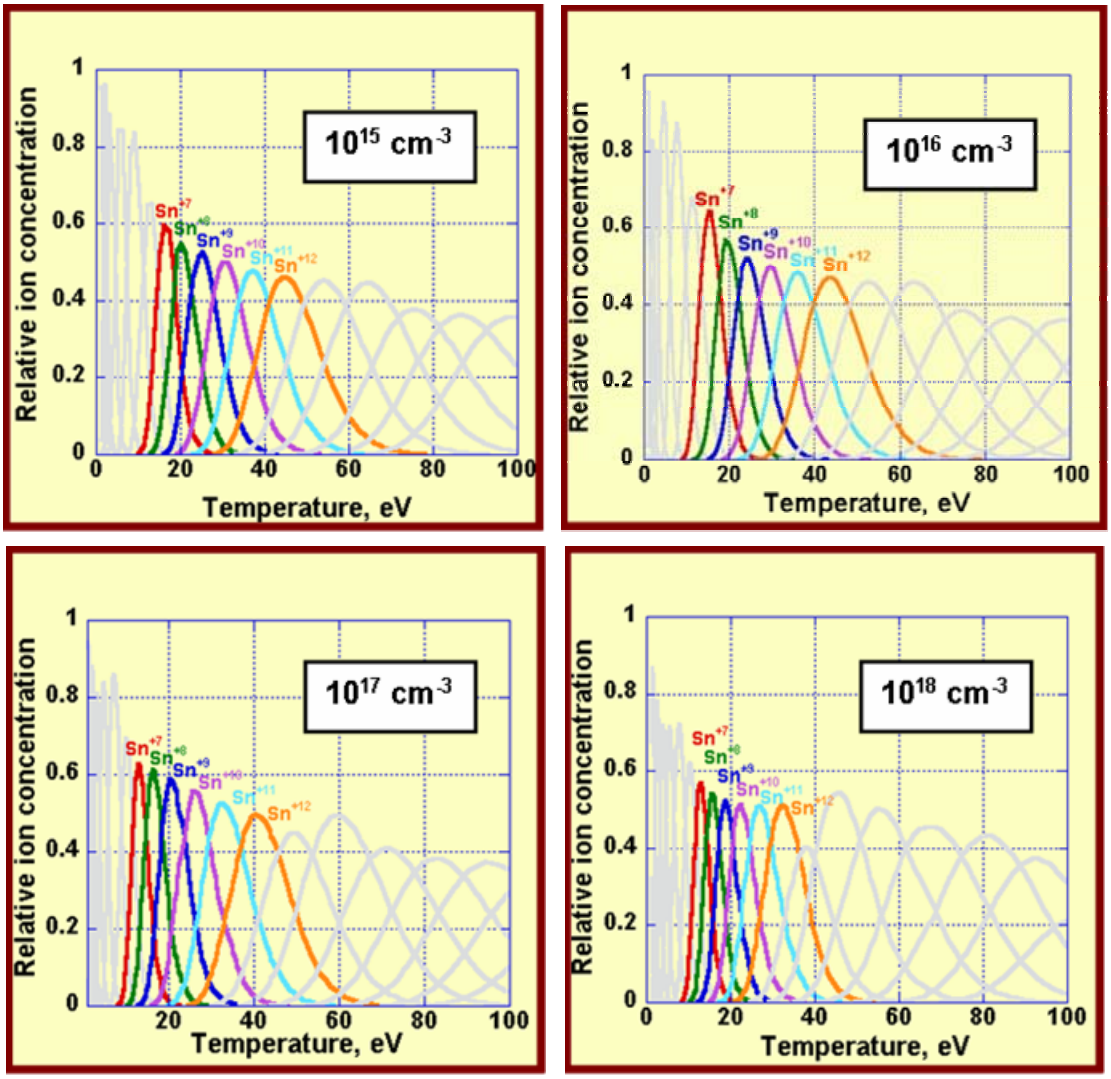

Fig. 1: Concentrations of tin ions for various densities

Our calculations can be validated and benchmarked by comparison to the results of other authors. Accordingly to the results calculated by the CRE model and reported in [14], the concentrations of xenon ions at $n_e = 10^{17}\,\mathrm{cm}^{-3}$ and $T_e = 32$ eV were 20% Xe+9, 25% Xe+10, 20% Xe+11, and 13% Xe+12, as shown by gray shading in the second column of Table 1. As seen from the other data in the table, our calculations generally agree with these figures, except that we obtained a twice larger value at $T_e = 31$ eV for the concentration of Xe+10 ions. We tend to rely on nearly 45% concentration of Xe+10, which would fix the total concentration of all ions to 100% and be more realistic in terms of the relative concentration of the major ion to the others.

The authors of Ref. 14 also reported ion concentrations at similar temperature and density

for a tin plasma to be 15% Sn+8, 40% Sn+9, 30% Sn+10, and 15% Sn+11. As shown in column 2 of Table 2, these results are similar to our computations for $T_e = 29$ eV. Results of the tables generally confirm the very complex composite nature of xenon and tin plasmas, where at the same conditions one may expect to find up to seven ion species.

Table 1: Concentration (in percent) of xenon ions at 10^{17} cm^{-3}. Top two rows give temperature and plasma density. Shaded data from Ref. 14.

T_e, eV	32	30.8	31.0	31.2	31.4	31.6	31.8	32.0	32.2	32.4
ρ_e, g/cm^3		2.19×10^{-6}	2.18×10^{-6}	2.17×10^{-6}	2.16×10^{-6}	2.16×10^{-6}	2.15×10^{-6}	2.14×10^{-6}	2.13×10^{-6}	2.13×10^{-6}
Xe+7		0.02	0.02	0.02	0.01	0.01	0.01	0.01	0.01	0.01
Xe+8		2.49	2.25	2.04	1.84	1.66	1.50	1.35	1.22	1.10
Xe+9	20	24.15	22.90	21.69	20.51	19.37	18.29	17.23	16.22	15.25
Xe+10	25	49.08	49.03	48.88	48.63	48.30	47.91	47.42	46.86	46.22
Xe+11	20	22.07	23.34	24.62	25.91	27.19	28.49	29.76	31.02	32.26
Xe+12	13	2.14	2.40	2.70	3.02	3.36	3.70	4.10	4.53	5.00
Xe+13		0.04	0.05	0.06	0.07	0.09	0.10	0.12	0.15	0.17

Table 2: Concentration (in percent) of tin ions at 10^{17} cm^{-3}. Top two rows give temperature and plasma density. Shaded data from Ref. 14.

T_e, eV	32	25	28	29	30	31	32	35
ρ_e, g/cm^3		2.37×10^{-6}	2.19×10^{-6}	2.14×10^{-6}	2.09×10^{-6}	2.05×10^{-6}	2.01×10^{-6}	1.91×10^{-6}
Sn+7		12.42	2.85	1.64	0.92	0.51	0.28	0.04
Sn+8	15	40.58	20.60	14.98	10.50	7.15	4.74	1.23
Sn+9	40	37.07	45.50	42.80	38.25	32.73	26.96	12.58
Sn+10	30	8.27	26.94	33.69	39.35	43.32	45.30	40.18
Sn+11	15	0.40	3.85	6.59	10.34	15.02	20.41	36.66
Sn+12		0.00	0.12	0.29	0.63	1.25	2.26	8.80

3. THERMODYNAMIC PLASMA PROPERTIES AND EQUATION OF STATE

After electron N_e and ion N_i concentrations are found by the CRE model, they can be substituted into a set of equations of state. Generally, the two-temperature approximation for pressure p contains the correspondent terms for kinetic energy of ions and electrons. The equation for internal energy e_{int} contains the terms for ionization and excitation of electrons:

$$P = kT_i \sum_i N_i + kT_e N_e,$$
$$e_{\text{int}} = \frac{3kT_e N_e}{2\rho} + \frac{3kT_i \sum_i N_i}{2\rho} + \frac{1}{\rho}\sum_i N_i \left(\left(\sum_{i-1} I_i \right) + \sum_j \frac{\varepsilon_{ji} N_{ji}}{N_i} \right). \quad \textbf{(3.1)}$$

Here we use traditional notation for Boltzmann's constant k, ionization potential I_i of the atomic level i, plasma density ρ, excitation energy of level j to level i ε_{ji}, electron and ion temperatures T_e, T_i. Results of these calculations are presented in Fig. 2.

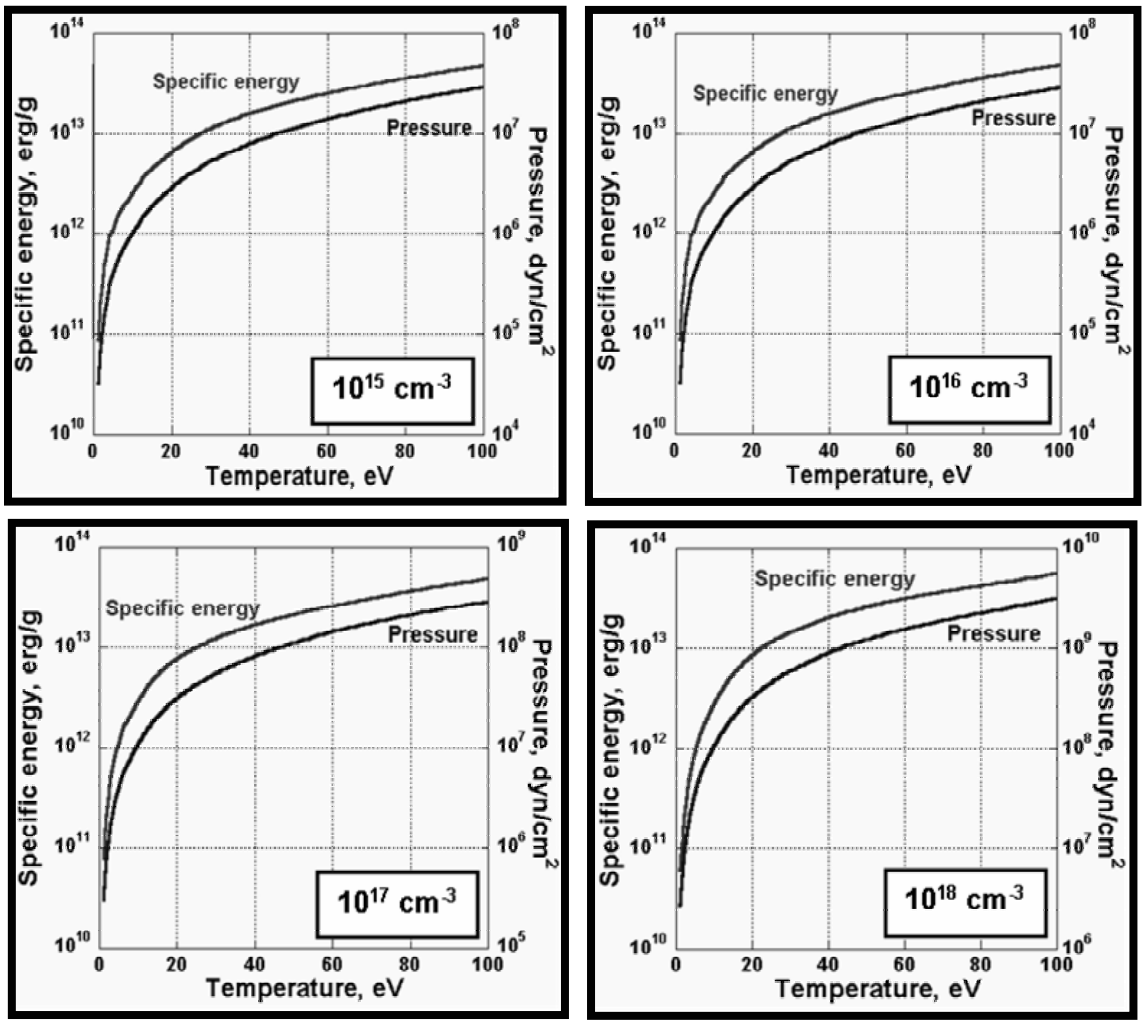

Fig. 2: Calculations from equation of state for tin ions at various densities

Reciprocal to the resistivity η, the electrical conductivity σ is found as the sum of conductivities defined by the electron scattering σ_c and σ_n on charged and neutral particles.

$$\eta = \frac{1}{\sigma} = \frac{1}{\sigma_c} + \frac{1}{\sigma_n}; \quad \sigma_c = \frac{4\sqrt{2}}{\pi\sqrt{\pi}} \frac{(kT_e)^{3/2}\beta}{e^2 Z\Lambda}; \quad \sigma_n = \frac{3}{2}\sqrt{\frac{2}{\pi}} \frac{N_e e^2}{\sqrt{m_e kT_e} N_0 s_0}. \tag{3.2}$$

Here we use standard notation for Coulomb logarithm Λ, concentration of neutral atom N_0, electron charge *e*, and mean ion charge *Z*. Parameter β is an electron-electron scattering correction [15]. Empirical values of transport crosssections s_0 are taken from [16].

4. DETAILED SET OPACITIES IN WIDE ENERGY RANGE

The electronic transitions and their accompanying absorption and emission of photons are subdivided into three types: bremsstrahlung; photoionization from ground, excited, and inner levels; and discrete transitions. The latter is approximated in the form of dipole transitions and includes transitions between ground and excited states, transitions between excited states, and partly the transitions from inner shells. Because of its importance, the profiles of spectral lines are processed very carefully by means of all major broadening mechanisms, such as radiation, Stark, Doppler, and resonance broadenings [17].

The total absorption coefficient κ_{abs} is calculated as a sum of absorption coefficients for free-free κ_{ff}, bound-free κ_{bf}, and bound-bound κ_{bb} radiation transitions weighed to the value of the population levels:

$$\begin{aligned}
\kappa_{ff}(T,\rho,\hbar\omega) &= \sum_i \sigma_i(T,\hbar\omega) n_i(T,\rho) n_e(T,\rho)\left(1-\exp(-\hbar\omega/kT)\right), \\
\kappa_{bf}(T,\rho,\hbar\omega) &= \sum_i \sum_j \sigma_{ij}(\hbar\omega) N_{ij}(T,\rho), \\
\kappa_{bb}(T,\rho,\hbar\omega) &= \sum_i \sum_{j,k} \frac{\pi e^2}{m_e c} f_{jk} \Phi(T,\rho,\omega) N_{ij}(T,\rho).
\end{aligned} \tag{4.1}$$

Knowing the crosssections of inverse processes, the total emission coefficient κ_{emi} is calculated by similar formulae. The values of electron density n_e and ion density n_i are calculated as described in previous section. The oscillator strengths f_{jk}, crosssections for photo absorption σ_i, crosssections for photoionization σ_{ij}, and line profile Φ are given elsewhere [5, 6, 8].

As shown earlier [5, 18], accounting for electrostatic and spin-orbit splitting of shells and spectral lines considerably influences the dynamics of the energy balance in the plasma. A method of calculating the optical coefficients for high-Z plasma was developed and implemented [5, 19] by means of the CRE model. The important feature of this method is the joint use of HFS atomic data and Racah techniques of angular moments. This feature makes possible the use of comparatively unsophisticated methods to consider the complex electronic structure of each

participating ion, and the complicated splitting of each configuration into terms (using the *LS*-coupling approximation), over a wide range of spectral frequencies, and in the expected range of temperatures and densities. By this technique, the detailed emission and absorption spectra are initially calculated over a very complete spectral frequency scale (up to 100,000 points) for the expected range of MHD values. The width of the frequency interval was comparable to the Doppler width of the strongest spectral lines, which provides a satisfactory resolution of the line profiles. In Fig. 3 we present calculated emission and absorption coefficients for the tin plasma at typical temperature and density (26 eV and 10^{16} cm^{-3}).

5. PLANCK GROUP AVERAGED OPACTITES IN WIDE ENERGY RANGE

Because of the large size of the generated opacity tables, the practical use of such detailed data is not convenient, and the emission and absorption coefficients are thus averaged in spectral groups. A rigorous theory for averaging the opacities within a group of frequencies does not exist. Such an averaging procedure is considered correct only when the absorption coefficient is constant within the group, or the optical thickness of each line is very small, and the absorption becomes a linear-like function from the frequency. This situation is only possible for a continuum, but even in that case, every photoionization threshold must become a boundary of a group. It becomes even more complicated for the lined spectrum, when the absorption coefficient often drops several orders of magnitude within a very limited frequency interval, say, from the center of a very strong spectral line to the wings of the same line, and the center of the line is optically thick. Moreover, the temperature and density values may vary. This change leads to spectral lines for the other ions, along with changes in the width of the existing lines.

From a practical viewpoint, an organized selection of the strongest lines is a reasonable way to describe the optical coefficients within the most important hydrodynamic areas for typical temperature and density values. The other lines are averaged within broad groups. Unfortunately, the primary goal of the numerical simulation is the determination of the typical hydrodynamic parameters within the important areas of the plasma domain!

For a uniform isothermal plasma, the optical thickness of a spectral line is determined by multiplying the absorption coefficient of the line by the linear dimension of the plasma $\tau(\varepsilon) = \kappa_{\text{abs}}(\varepsilon) \cdot l$. In the case of a nonuniform nonisothermal plasma, this definition is generalized as $\tau(\varepsilon) = \int \kappa_{\text{abs}}(T, \rho, \varepsilon)\, dl$ over the interval Δl, where the ion exists emitting with frequency ε.

The borders of the groups are calculated from the following considerations. First, the width of a group $\Delta\varepsilon$ should never exceed αT, where T is the plasma temperature, and α is a chosen parameter for averaging. This condition provides the smooth averaging of opacities in the continuum region, where the averaging is normally performed within the broad groups, and the optical thickness is much less than one. Second, invariability of the optical coefficient is required for a chosen value β within the group. This condition provides a very specified resolution of the spectral lines with the optical thickness nearly at unity, and the wings of the lines with the optical thickness greater than unity. A final consideration is that all those

frequencies which belong in the detailed spectrum to a line with $\tau(\varepsilon) \geq 1$ are also included in the domain of the groups. This condition provides a very thorough resolution of the strong lines in the averaging spectrum. By variation of the parameters α and β, several group mean opacities are generated with different levels of completeness and detail.

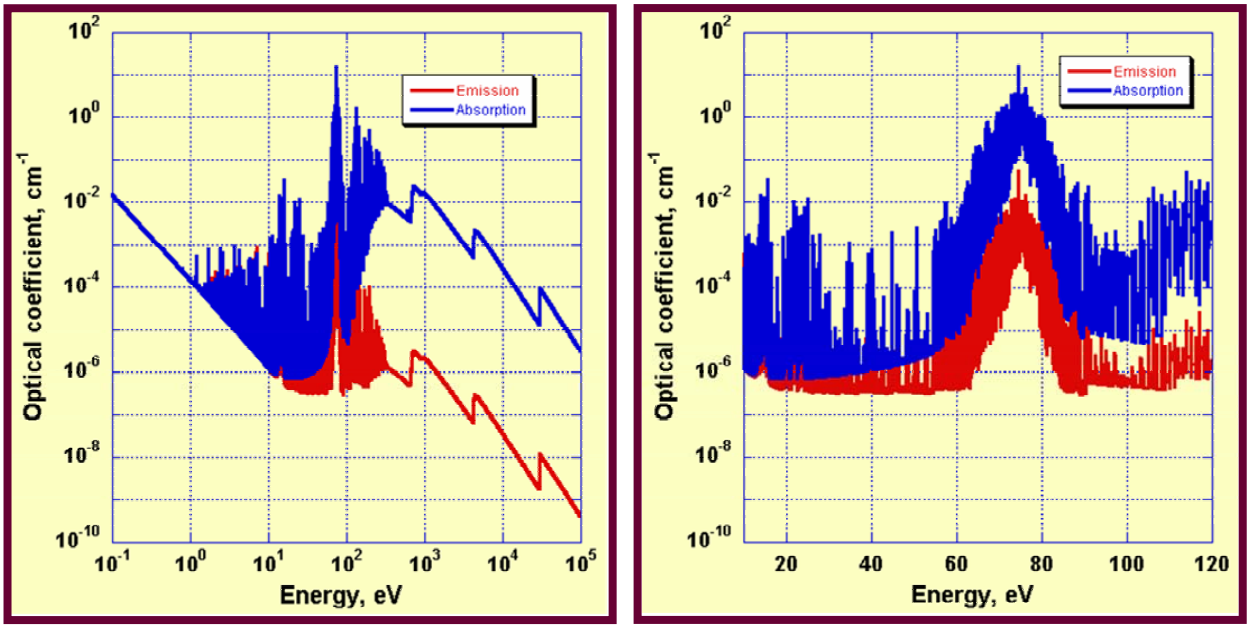

Fig. 3: Optical coefficients for tin plasma at T = 26 eV and N = 10^{16} cm^{-3}

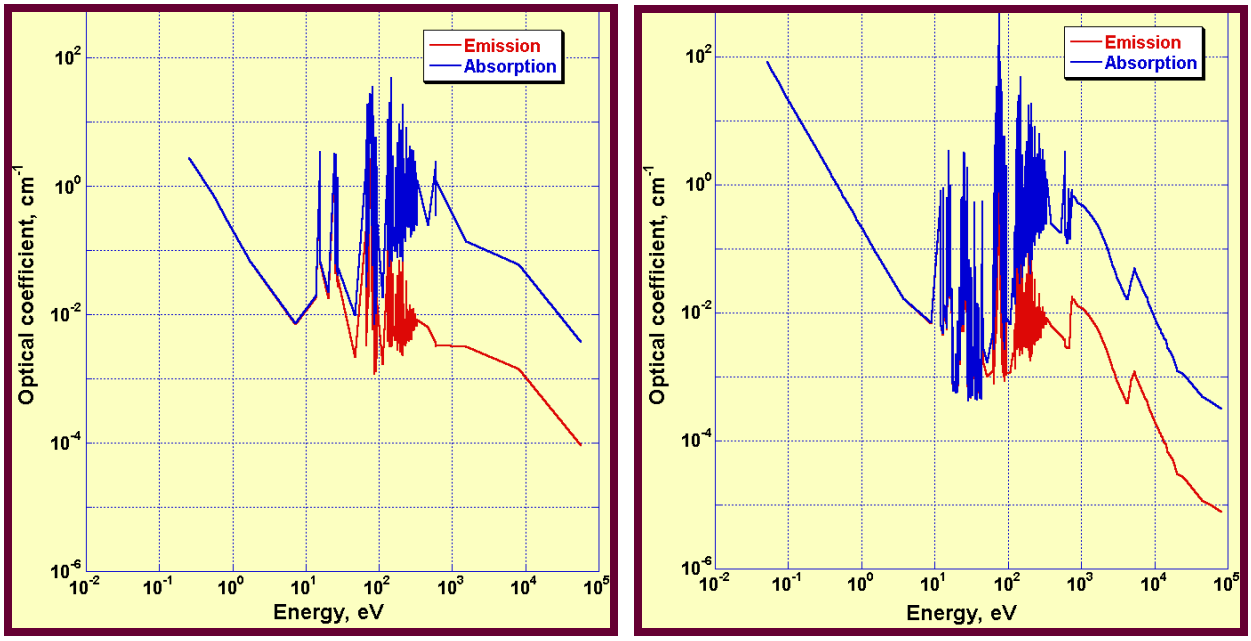

Fig. 4: Planck mean optical coefficients for tin plasma, averaged over 691 (left) and 3240 (right) groups

Based upon several recent studies [3, 4], it is supposed that the maximal radiation flux corresponds to the moment of pinch formation. Typical tin pinch parameters are the following: the temperature is close to 25 eV, the density is $3 \cdot 10^{17}$ cm^{-3}, the spectral range in radiation energies varies from 5 eV to 250 eV, and the average optical plasma thickness is 1 cm. Using these parameters, we have generated a basic set of opacities, averaged within 691 spectral groups. Taking a wider set of temperature and density pairs, we have generated the optimal scale of spectral groups. Combining all scales, the resulting energy scale has a total of 3240 energy groups. Results of the Planck mean absorption and emission coefficients for the mentioned temperature and density values are shown in Fig. 4 above. As the next step, the output of the self-consistent hydrodynamic/radiation transport calculations with these opacities can be used for further improvements in the quality of the coefficients.

6. HF ENERGY LEVELS AND OTHER DATA FOR EUV EMITTING TIN ION SPECIES

The accuracy of the HFS model is typically within several percents for the split levels, which is insufficient for the narrow 2% bandwidth. To obtain a higher accuracy of the EUV optical coefficients, we use the *LSD* HF method, which is more accurate but significantly more advanced and difficult to implement. Strictly speaking, the HF method encompasses several methods for calculation of various atomic structures. Being applied to the same atomic system, each modification of the HF method can produce different results, so the choice of the appropriate method is very important in terms of the overall accuracy of the calculations.

In the HF method the wavefunctions, eigenvalues, and total energy of an atom are found from the variational principle for the well-known Schrödinger equation:

$$\hat{H}\Psi = E\Psi\,, \tag{6.1}$$

where $\hat{H}$ is a Hamiltonian of the atom, including the interaction of each electron with the nucleus and the other electrons; E is the total energy of an atom; and Ψ is the atomic wavefunction, which is expressed through the atomic orbitals $\varphi_i(r_j) \equiv \varphi_{n_i l_i}(r_j)$ as

$$\Psi = \begin{vmatrix} \varphi_1(r_1) & \varphi_1(r_2) & \cdots & \varphi_1(r_n) \\ \varphi_2(r_1) & \varphi_2(r_2) & \cdots & \varphi_2(r_n) \\ \cdots & \cdots & \cdots & \cdots \\ \varphi_n(r_1) & \varphi_2(r_2) & \cdots & \varphi_n(r_n) \end{vmatrix}. \tag{6.2}$$

The number of the atomic orbitals is determined by the number of shells in the atom. For instance, the tin atom has $1s^2\ 2s^2\ 2p^6\ 3s^2\ 3p^6\ 3d^{10}\ 4s^2\ 4p^6\ 4d^{10}\ 5s^2\ 5p^2$ ground state, or 11 orbitals. Each orbital is found from the system of integral-differential equations for functions φ_{nl}:

$$\left\{-\frac{1}{2}\frac{d^2}{dr^2}+\frac{l(l+1)}{2r^2}-\frac{Z}{r}+\frac{2}{N_{nl}}\sum_x f_x(nl)y^x_{nl,nl}(r)+\frac{1}{N_{nl}}\sum_{n'l'}\sum_x \alpha_x(nl,n'l')y^x_{n'l',n'l'}(r)-\varepsilon_{nl}\right\}\varphi_{nl}(r)-$$

$$-\frac{1}{N_{nl}}\sum_{n'l'}\sum_x \beta_x(nl,n'l')y^x_{n'l',nl}(r)\varphi_{n'l'}(r)-\sum_{n'}\varepsilon_{nl,n'l'}\varphi_{n'l'}(r)=0.$$

The expressions for the radial integrals $y^x_{n'l',nl}(r)$, as well as the potentials $f_x y^x_{nl,nl}(r)$, $\alpha_x y^x_{n'l',n'l'}(r)$, and $\beta_x y^x_{n'l',nl}(r)$, are omitted here and can be found elsewhere [6]. Here, we just note that they define the interaction of the electrons of the *nl* shell with the other electrons of the same shell, averaged over all angles, and with the electrons of the other shells, including both the usual and the exchange interactions.

In general, the coefficients f_x, α_x, and β_x depend on the whole set of quantum numbers, defining the atomic level under consideration, and particularly on *L* and *S*. Consequently, different orbitals (or radial wavefunctions) φ_{nl}, $\varphi_{n'l'}$, … correspond to different terms of various electron configurations.

In a well-known monograph [8], Cowan introduces the concept of the *LS*-dependent Hartree-Fock (*LSD* HF) calculations. His approach uses a different set of radial wavefunctions for each *LS* term, assuming the pure *LS*-coupling scheme. To be precise, the method should be called *LSvD* HF, because the total energy for *d*-shells also depends on the seniority number v. The number of terms can be large, especially for *d*- and *f*-shells. Significant simplification can be gained by assuming that for all terms the wavefunctions and eigenvalues are identical and calculated for the center of gravity of the shell. The so-called "average term approximation" works very well for the highly excited states, but is quite unpredictable for the outer and inner shells. In contrast to the average term HF, all *LSD* HF wavefunctions, eigenfunctions, and Slater integrals depend on the *L* and *S* quantum numbers for inner and outer shells. This condition requires longer, but more accurate computations, and very important for calculation the total energies of the atomic levels. Table 3 presents our calculations of the energies of the Xe XI inner shells by the *LSD* HF method. These are compared to the results obtained by the well-known Cowan HF average term code, which is widely used in spectroscopic research for identification of atomic levels. The correspondence is within 1-5%, although our results are consistently lower than those from the Cowan code for the inner shells, and slightly higher for the open shell. Similar results for Sn VIII are presented in Table 4, and the energies for the Sn VIII – Sn XIII, calculated by various methods are shown in Appendix A.

The angular wavefunctions are normally calculated separately to the radial wavefunctions by the summation of the electron momentums. As a rule, the two limited cases are rarely realized in practice, that is, when electrostatic interaction is considered predominant (*LS*-coupling) or spin-orbit interaction exceeds the electrostatic interaction (*jj*-coupling). In such intermediate cases, the Hamiltonian matrix cannot be written diagonal in any coupling schemes. Therefore, the complete matrix is written by transforming the Coulomb matrix from *LS*-representation to *jj*-representation. The eigenvalues of the Hamiltonian matrix are found later by numerical diagonalization, and the eigenvector (purity vector) defines the composition of the level, corresponding to this eigenvalue. The level is normally assigned according to the highest

contribution of the basis term from the purity vector. Note that the energy levels, found within the intermediate coupling, never have 100 percent pure *LS*- or *jj*-coupling, and the difference always exists between the level assigned within the intermediate coupling or the level calculated within the pure coupling scheme and accordingly assigned as required by the scheme.

The relativistic effects can be negligible for the low-Z elements, but apparently become evident for intermediate-Z and high-Z elements. The most widespread and relatively easy way to account for them within the HF method is by one-electron relativistic corrections within the framework of perturbation theory. The more strict and accurate way to account for relativistic effects is to use the Dirac-Fock approximation, but this significantly complicates the problem, while the gain from it would be pronounced only for the high-Z elements.

Table 3: Energies of Xe XI inner shells by *LSD* HF and average term HF.

	HEIGHTS-ATOM					Cowan
Conf	^1S	^2P	^1D	^3F	^1G	E_{av}
$1s^2$	2462.1420	2462.1173	2462.1165	2462.1075	2462.1211	2565.4407
$2s^2$	391.7600	391.7356	391.7349	391.7260	391.7394	417.8558
$2p^6$	365.3100	365.2854	365.2847	365.2757	365.2892	376.5671
$3s^2$	92.9495	92.9293	92.9289	92.9216	92.9325	98.5881
$3p^6$	81.8833	81.8629	81.8625	81.8551	81.8661	84.8207
$3d^{10}$	63.3815	63.3609	63.3605	63.3530	63.3642	64.1559
$4s^2$	27.4180	27.4061	27.4061	27.4018	27.4080	28.6868
$4p^6$	23.1245	23.1133	23.1132	23.1092	23.1151	23.9933
$4d^8$	17.0287	17.1508	17.1568	17.2021	17.1329	17.0272

Table 4: Energies of Sn VIII inner shells by *LSD* HF and average term HF.

	HEIGHTS-ATOM								Cowan
Conf	^2P	^4P	$^2{}_1D$	$^2{}_3D$	^2F	^4F	^2G	^2H	E_{av}
$1s^2$	2091.3064	2091.3013	2091.3279	2091.3127	2091.3169	2091.2909	2091.3029	2091.3064	2165.7804
$2s^2$	322.6554	322.6503	322.6769	322.6617	322.6659	322.6399	322.6520	322.6554	341.0976
$2p^6$	298.6029	298.5977	298.6244	298.6092	298.6134	298.5873	298.5994	298.6029	307.0733
$3s^2$	71.5397	71.5351	71.5580	71.5449	71.5484	71.5264	71.5367	71.5397	75.3565
$3p^6$	61.7069	61.7023	61.7253	61.7121	61.7157	61.6935	61.7039	61.7069	63.8827
$3d^{10}$	45.3449	45.3404	45.3633	45.3502	45.3537	45.3315	45.3419	45.3449	46.0725
$4s^2$	18.6978	18.6948	18.7092	18.7009	18.7030	18.6896	18.6961	18.6978	19.4893
$4p^6$	15.0560	15.0532	15.0665	15.0589	15.0608	15.0484	15.0544	15.0560	15.6992
$4d^7$	10.2634	10.2836	10.1689	10.2343	10.2149	10.3322	10.2796	10.2634	10.1565

As follows from Tables 3 and 4, it is very hard to benchmark and verify the accuracy of the computation of such complicated elements as xenon or tin without experimental results. Before proceeding with our tin calculation, we checked the accuracy of our code on well-known elements with available experimental measurements of the levels for oxygen (Table 5) and argon (Table 6). The NIST tables are published in Ref. 20. The simplicity of oxygen and argon comes from the pronounced *LS*-coupling approximation, which allows us to uniquely identify and assign the levels once the intermediate coupling is applied. The average term HF method presents similar, but slightly less accurate results, despite the fact that the average term approximation is expected to work very well for the excited states [8].

As mentioned above, the intermediate-Z elements, such as tin, do not have any pure

coupling scheme, and the intermediate coupling approximation is the only reasonable choice in computer calculation of atomic levels. However, the assignment of the calculated levels is arbitrary, preserving only the exact quantum number of total momentum *J*. In column 3 of the Table 7, we present our results for the Sn VIII energy levels, and in the column 7 of the same table are the results of the Cowan code. We have ordered the levels by increasing the total moment and arranged the Cowan code levels accordingly to our identification. Since different intermediate coupling codes might have different naming schemes, the reasonable way of presenting the results is arranging the levels accordingly to the total moment of the level. The experimental energy levels are available thanks to the Ref. 23, and we can benchmark the accuracy of these calculations. As one can see, the energy levels computed by us are close to the Cowan code results and differ from the experimentally defined values from 3% to 12%.

Table 5: O I $2p^3$ 3s excited state energy levels (in cm^{-1}).

Excited level	HEIGHTS-ATOM		Cowan		NIST Tables
	Level	Acc,%	Level	Acc	
$2p^3(^2P)3s(^2S)^3P_0$	51017.20		56245.60		
$2p^3(^4S)3s(^2S)^3S_1$	2693.72	11.00	9454.00	212.35	3026.78
$2p^3(^2P)3s(^2S)^1P_1$	52458.82		60975.40		
$2p^3(^2P)3s(^2S)^3P_1$	51017.20		56247.20		
$2p^3(^2D)3s(^2S)^3D_1$	31117.88	13.62	34690.20	26.67	27387.22
$2p^3(^4S)3s(^2S)^5S_2$	0.00	0.00	0.00	0.00	0.00
$2p^3(^2P)3s(^2S)^3P_2$	51024.33		56250.60		
$2p^3(^2D)3s(^2S)^1D_2$	32506.93		39418.50		
$2p^3(^2D)3s(^2S)^3D_2$	31114.91	13.64	34691.10	26.71	27379.33
$2p^3(^2D)3s(^2S)^3D_3$	31117.88	13.70	34693.20	26.77	27367.21

Table 6: Ar II $3p^4$ 3d excited state energy levels (in cm^{-1}).

Excited level	HEIGHTS-ATOM		Cowan		NIST Tables
	Level	Acc,%	Level	Acc	
$3p^4(^1D)3d(^2_1D)^2S_{0.5}$	40846.4178	21.09	52850.1	2.1	51765.7720
$3p^4(^1D)3d(^2_1D)^2P_{0.5}$	41248.8245	2.93	18681.8	56.0	42493.6398
$3p^4(^3P)3d(^2_1D)^2P_{0.5}$	35121.2034	183.63	93017.9	651.2	12382.6192
$3p^4(^3P)3d(^2_1D)^4P_{0.5}$	18092.2789	21.42	22836.6	53.3	14900.6902
$3p^4(^3P)3d(^2_1D)^4D_{0.5}$	394.0666	3.97	403.8	1.6	410.3420
$3p^4(^1S)3d(^2_1D)^2D_{1.5}$	58824.3505	23.57	63587.7	33.6	47604.4745
$3p^4(^1D)3d(^2_1D)^2P_{1.5}$	41249.8121	1.98	19756.3	53.1	42082.5271
$3p^4(^1D)3d(^2_1D)^2D_{1.5}$	40839.6141	0.83	24700.9	39.0	40502.2899
$3p^4(^3P)3d(^2_1D)^2P_{1.5}$	35483.3365	165.96	92456.2	593.0	13341.5221
$3p^4(^3P)3d(^2_1D)^4P_{1.5}$	18366.1832	21.02	23196.9	52.9	15175.7514
$3p^4(^3P)3d(^2_1D)^2D_{1.5}$	37436.7702	106.29	103522.9	470.4	18147.6279
$3p^4(^3P)3d(^2_1D)^4D_{1.5}$	291.3525	3.96	299.0	1.4	303.3660
$3p^4(^3P)3d(^2_1D)^4F_{1.5}$	12253.5961	10.95	15783.3	42.9	11044.0744
$3p^4(^1S)3d(^2_1D)^2D_{2.5}$	58824.2407	24.46	63853.6	35.1	47264.8629
$3p^4(^1D)3d(^2_1D)^2D_{2.5}$	41036.0439	2.57	25648.1	35.9	40008.2352
$3p^4(^1D)3d(^2_1D)^2F_{2.5}$	37712.7595	21.76	46206.2	49.2	30972.1990
$3p^4(^3P)3d(^2_1D)^4P_{2.5}$	18690.6764	20.21	23679.7	52.3	15548.5860
$3p^4(^3P)3d(^2_1D)^2D_{2.5}$	36402.7156	94.04	102099.4	444.2	18759.9507
$3p^4(^3P)3d(^2_1D)^4D_{2.5}$	110.3957	28.24	152.4	0.9	153.8450
$3p^4(^3P)3d(^2_1D)^2F_{2.5}$	22225.5343	24.72	29109.4	63.3	17820.3401
$3p^4(^3P)3d(^2_1D)^4F_{2.5}$	11921.9700	10.59	15500.2	43.8	10780.3183
$3p^4(^1D)3d(^2_1D)^2F_{3.5}$	37159.2445	19.18	46532.6	49.2	31179.1749
$3p^4(^1D)3d(^2_1D)^2G_{3.5}$	26396.3199	20.66	29245.5	33.7	21876.6617
$3p^4(^3P)3d(^2_1D)^4D_{3.5}$	0.0000	0.00	0.0	0.0	0.0000
$3p^4(^3P)3d(^2_1D)^2F_{3.5}$	21387.5803	26.92	27647.0	64.1	16851.8825
$3p^4(^3P)3d(^2_1D)^4F_{3.5}$	11623.0456	11.87	15081.4	45.2	10389.7346
$3p^4(^1D)3d(^2_1D)^2G_{4.5}$	26396.3199	20.66	29074.2	32.9	21876.6617
$3p^4(^3P)3d(^2_1D)^4F_{3.5}$	11120.1196	12.79	14509.5	47.2	9858.9536

From a theoretical standpoint, the agreement of the calculated atomic energy levels with the experimentally measured values within 3% to 12% may be considered encouraging, but in reality, the required EUV bandwidth has much greater restrictions. The well-known effect of overestimation of the theoretical energy-level splitting results in slightly larger values of Coulomb electron-electron interactions [8, 21]. The electron correlation cannot be determined scaled-down theoretical values of the single-configuration Slater integrals. Any experimental data can actually be a great help in determining the exact values of the scaling factors, as demonstrated in Table 8. The experimental values in the second column are taken from Ref. 22. As expected, the purely theoretical values for the ground energy levels of Xe XI, shown in column 3, are slightly overestimated, by approximately 10%, but scaling the Slater integrals to a factor of 0.82 yields a very accurate result, within less than 2% for most ground levels. Thanks to the Ref. 22, we can also benchmark the accuracy of our calculation for the Xe XI $4d^7$ 5p excited levels. Additionally, we have calculated the same energy levels by the Cowan code. The calculated results for Xe XI $4d^7$ 5p excited levels in Table 9 show excellent agreement with the experimental values, as accurate as 1-2% for most levels. As evident from the table, the Cowan code produces slightly higher energy values, which would shift the $4d^8$–$4d^7$5p transition array toward longer wavelengths.

Table 7: Sn VIII $4d^7$ ground state energy levels.

	Exp	HEIGHTS-ATOM (th)		HEIGHTS-ATOM (fit)		Cowan	
	cm^{-1}	Energy, cm^{-1}	Acc	Energy, cm^{-1}	Acc	Energy, cm^{-1}	Acc
$4d^{72}\,{}^3P_{0.5}$	35458	36645	3.35%	36451	2.80%	37684	6.28%
$4d^{74}\,{}^3P_{0.5}$	23946	24936	4.13%	23326	2.59%	25937	8.32%
$4d^{72}\,{}^3P_{1.5}$	30657	32889	7.28%	32137	4.83%	32347	5.51%
$4d^{74}\,{}^3P_{1.5}$	18280	19072	4.33%	18259	0.12%	20472	11.99%
$4d^{72}\,{}^1D_{1.5}$	-	69434		70831		75845	
$4d^{72}\,{}^3D_{1.5}$	44177	43707	1.06%	43468	1.60%	45637	3.31%
$4d^{74}\,{}^3F_{1.5}$	12153	13375	10.06%	12823	5.25%	12083	0.58%
$4d^{74}\,{}^3P_{2.5}$	20373	21448	5.28%	19525	4.16%	22171	8.83%
$4d^{72}\,{}^1D_{2.5}$	75377	65418	13.21%	66819	11.35%	79115	4.96%
$4d^{72}\,{}^3D_{2.5}$	33670	42009	24.77%	41517	23.30%	34785	3.31%
$4d^{72}\,{}^3F_{2.5}$	45452	45232	0.48%	44567	1.95%	48749	7.25%
$4d^{74}\,{}^3F_{2.5}$	10341	11157	7.89%	10605	2.49%	10120	2.13%
$4d^{72}\,{}^3F_{3.5}$	49476	49870	0.80%	48753	1.46%	52498	6.11%
$4d^{74}\,{}^3F_{3.5}$	6986	7130	2.05%	6716	3.87%	6704	4.03%
$4d^{72}\,{}^3G_{3.5}$	29001	28378	2.15%	29338	1.16%	29358	1.23%
$4d^{74}\,{}^3F_{4.5}$	0	0		0		0	
$4d^{72}\,{}^3G_{4.5}$	22636	21884	3.32%	22976	1.50%	23082	1.97%
$4d^{72}\,{}^3H_{4.5}$	37751	36996	2.00%	37413	0.89%	38072	0.85%
$4d^{72}\,{}^3H_{5.5}$	30312	29369	3.11%	30042	0.89%	30933	2.05%

Table 8: Xe XI $4d^8$ ground state energy levels (in cm^{-1}).

	Exp	Theor	Acc,%	Modified	Acc,%
$4d^8\ ^3F_4$	0	0		0	
$4d^8\ ^3F_3$	13140	15069	14.68	13184	0.34
$4d^8\ ^3F_2$	15205	15456	1.65	15219	0.09
$4d^8\ ^3P_2$	26670	29402	10.24	27025	1.33
$4d^8\ ^3P_0$	32210	37699	17.04	32410	0.62
$4d^8\ ^3P_1$	34610	39394	13.82	35145	1.54
$4d^8\ ^1G_4$	40835	45551	11.55	39917	2.25
$4d^8\ ^1D_2$	42900	46204	7.7	43006	0.25
$4d^8\ ^1S_0$	88130	99330	12.71	85587	2.89

Table 9: Xe XI $4d^7$ 5p excited state energy levels (in cm^{-1}).

J	HEIGHTS	Exp	Acc,%	Cowan	Exp	Acc,%
J = 0	753682			704730		
	764819			724612		
	767530			727272		
	776382			737419		
	789881	792311	0.31	757151		
	796489			758364		
	835707			771196	792311	2.74
J = 1	542235	742594	36.95	693853		
	757317	745470	1.56	702217		
	765462	752155	1.74	710994		
	771635	754745	2.19	722192		
	777881	758337	2.51	724441	742594	2.51
	779903	760950	2.43	730621	745470	2.03
	781248	765770	1.98	735493	752155	2.27
	785224	767369	2.27	738123	754745	2.25
	788088	775030	1.66	739352	758337	2.57
	792118	778350	1.74	745760	760950	2.04
	793228	784035	1.16	746488	765770	2.58
	795405	788396	0.88	754717	767369	1.68
	802074	791805	1.28	763654	775030	1.49
	807341	808130	0.10	768242	778350	1.32
	812504			771542	784035	1.62
	821941			788076	788396	0.04
	841501	830260	1.34	798662	791805	0.86
	843731			801863	808130	0.78
	846356			810811	830260	2.40
J = 2	691417			687857		
	724852	715730	1.26	692334		
	728526	721001	1.03	696514		
	732116	740757	1.18	700235		
	746236	746552	0.04	717679	715730	0.27
	749293	750512	0.16	718894		
	753451	753795	0.05	725032	721001	0.56
	758428	756170	0.30	726551		
	761149	762105	0.13	729295		
	767927	765052	0.37	732909		
	769318	766625	0.35	735891	740757	0.66
	773092	773315	0.03	738595	746552	1.08
	779656			741586	750512	1.20
	780705	781822	0.14	744032	753795	1.31
	783294			746840	756170	1.25
	786437	786580	0.02	752933	762105	1.22
	789616	788145	0.19	755918	765052	1.21
	790623			760587	766625	0.79
	793917	795995	0.26	764895	773315	1.10
	798349			767897	781822	1.81
	804334	802905	0.18	774832	786580	1.52
	809562			782382	788145	0.74
	815205	828875	1.68	783192	795995	1.63
	868819			808808	802905	0.73
	981088			815096	828875	1.69
J = 3	723800	709285	2.01	694244		
	730113	714855	2.09	699416	709285	1.41
	736320	725825	1.43	704967	714855	1.40
	743547	733755	1.32	712164	725825	1.92

J	HEIGHTS	Exp	Acc,%	Cowan	Exp	Acc,%
J = 3	748359	739322	1.21	717807	733755	2.22
	752695	741800	1.45	720466	739322	2.62
	758000	744955	1.72	723565	741800	2.52
	763470	746445	2.23	724781	744955	2.78
	771677	749351	2.89	728734	746445	2.43
	773934	752054	2.83	731322	749351	2.47
	774880	754860	2.58	733156	752054	2.58
	777965	759110	2.42	738201	754860	2.26
	781014	761266	2.53	739969	759110	2.59
	785056	766860	2.32	745423	761266	2.13
	790166	768773	2.71	747692	766860	2.56
	792063	773715	2.32	752379	768773	2.18
	792759	775570	2.17	754544	773715	2.54
	797858	780503	2.18	759955	775570	2.05
	801299	788465	1.60	767977	780503	1.63
	810423	795135	1.89	774072	788465	1.86
	813769	801225	1.54	781651	795135	1.73
	826715	824474	0.27	789720	801225	1.46
	830391	838289	0.95	804178	824474	2.52
	859482			818639	838289	2.40
J = 4	720948	695376	3.55	674946		
	729055	712223	2.31	691130	695376	0.61
	733795	725053	1.19	703565		
	737916	731458	0.88	709989		
	740340	737388	0.40	714976	712223	0.38
	757762	739542	2.40	718830		
	761448	744537	2.22	721907	725053	0.44
	763104	752285	1.42	731022	731458	0.06
	766332	755831	1.37	733091	737388	0.59
	773027	756016	2.20	734544	739542	0.68
	775476	763070	1.60	741653	744537	0.39
	780864	773968	0.88	750301	752285	0.26
	786082	775775	1.31	752696	755831	0.42
	799561			754242	756016	0.24
	801886			761942	763070	0.15
	804653			769559	773968	0.57
	826400			775551	775775	0.03
	830536			805690		
J = 5	683225	722439	5.74	677821		
	732407	730345	0.28	699866	722439	3.23
	739736	738248	0.20	709556	730345	2.93
	746958	740348	0.88	714977	738248	3.25
	763685	753352	1.35	719344	740348	2.92
	769708	759260	1.36	731954	753352	2.92
	771325	766947	0.57	737152	759260	3.00
	773197	767700	0.71	744858	766947	2.97
	785525	773968	1.47	751356	767700	2.18
	814311	789029	3.10	766642	773968	0.96
	823737			775264	789029	1.78
J = 6	730685			700419		
	765587			719093		
	768696			731718		
	774523			749845		
	782724			755705		
7	775010			739827		

The results, presented in Table 7 above were calculated in two steps. In the first step, we obtained the total energies of the ion by a pure analytical method. Results of this calculation are presented in column 3, and their relative accuracy compared to the measurements in Ref. 23 is shown in column 4. As expected, the pure theoretical method does not allow us to obtain an accuracy of 2% for the atomic levels of such a complicated ion as Sn VIII. We have shaded those levels for which the calculations are not accurate enough. In the second step, we used the experimentally defined values and found that at $F_f^2(dd) = 0.82 \cdot F_t^2(dd)$, $F_f^4(dd) = 0.91 \cdot F_t^4(dd)$, and $\zeta_f(d) = 0.96 \cdot \zeta_t(d)$ our values agree noticeably better, as shown by columns 5 and 6 in Table 7. In the formulas above, the subscript *f* means fit value, and the subscript *t* means theoretical value. At last, we have calculated the same levels by the Cowan code, which despite being purely theoretical, is still utilizing scaling factors near 10%, depending upon the nuclear charge of the element [8]. Our calculations for the excited Sn VIII $4d^6\ 5p^1$ energy levels are presented in Appendix B. Experimental values are taken from Ref. 23, and the fit values were determined as $F_f^2(dd) = 0.57 \cdot F_t^2(dd)$, $F_f^4(dd) = 2.11 \cdot F_t^4(dd)$, $\zeta_f(d) = 0.44 \cdot \zeta_t(d)$, $\zeta_f(p) = 0.35 \cdot \zeta_t(p)$, $F_f^2(pd) = 0.76 \cdot F_t^2(pd)$, and $G_f^3(pd) = 1.14 \cdot G_t^3(pd)$. As before, the theoretical values agreed with the experimental data within 5%, and once the experimental values are taken into account, the accuracy of our numerical simulation becomes less than 1% in most cases.

In sum, our calculated results compare favorably with available experimental data and a Cowan-average-term Hartree-Fock code, as well as other atomic codes with relativistic corrections. At the same time, the accuracy of the purely theoretical methods is not within the required 2%, so without the experimental values, one cannot guarantee the calculation of accurate EUV transitions. We have attained an accuracy within 3-7% of our purely theoretical calculations for Sn ions which lack experimental energy values. Once the energy levels are obtained, we can significantly improve our calculations to practically as accurate as the measured data.

7. DETAILED TIN EUV TRANSITIONS

Emission of light takes place when an atom changes from a state of higher energy to a state of lower energy. Similarly, absorption results in an upward transition that is caused by the action of the radiation field on an atom. The energy of a transition from state *i* to state *j* is formally defined as the difference of total energies of the atom or the ion in states *i* and *j*. As well known from the literature [6 - 8], the following are equivalent measures of total strength of the spectrum line: the probability of a transition W_{ij}, the radiation intensity of a spectrum line I_{ij}, and the weighted spontaneous-emission transition probability $g_j A_{ji}$, expressed through the statistical weight of the level $g_j = 2J + 1$ and the Einstein spontaneous emission transition probability rate A_{ji}. In our study, we normally use the non-dimensional (absorption) oscillator strength, which is related to the line strength S by the following expression:

$$f_{ij} = \frac{1}{3}\frac{\left(E_j - E_i\right)}{2J+1} S. \tag{7.1}$$

As above, unless otherwise stated, we use atomic units. The energy of the transition $\left(E_j - E_i\right)$ is given in Rydberg units, $2J+1$ is the degeneracy of the initial level, and the line strength is defined by the matrix element of the wavefunctions of the initial and final states with the electric dipole operator.

Using as before the intermediate coupling approximation, one can determine the wavefunctions of both states in the form of a linear combination of *LS*-coupled basic functions, where the coefficients of the components are obtained from the energy eigenvectors for the correspondent states. This allows us to represent the line strength in the form of the two dot products of the two component vectors to the dipole-transition matrix. Such a technique reduces the problem of calculating the line-strength matrix elements with uncoupled states to the matrix elements with the *LS*-coupled basis functions. The mathematical expressions for the matrix elements are rather complex and lengthy, so we direct the reader to the more complete theoretical publications [7, 24, 25]. Using traditional atomic theory notation for 6j- and 9j-symbols, fractional parentage coefficients, and square brackets, we only present the final expressions for calculation of the line strengths of typical transitions:

$$\begin{aligned} D_{LS}\left(l_1^n l_2^{k-1} - l_1^{n-1} l_2^k\right) &= \delta_{SS'}(-1)^{k+l_2+L_2+L'_2+L+S'_1+S'_2-J'}\left(nk[L_1,S_1,L'_2,S'_2,L,L',J,J']\right)^{0.5}\times \\ &\times \begin{Bmatrix} L & S & J \\ J' & 1 & L' \end{Bmatrix}\begin{Bmatrix} S'_1 & S'_2 & S \\ S_2 & S_1 & s \end{Bmatrix}\begin{Bmatrix} L_1 & L'_1 & l_1 \\ L_2 & L'_2 & l_2 \\ L & L' & 1 \end{Bmatrix}\times \\ &\times \left(l_1^n \alpha_1 L_1 S_1 \{l_1^{n-1}\alpha'_1 L'_1 S'_1\}\right)\left(l_2^{k-1}\alpha_2 L_2 S_2 \{l_2^k \alpha'_2 L'_2 S'_2\}\right) P^{(1)}_{l_1 l_2}, \end{aligned} \tag{7.2}$$

$$\begin{aligned} D_{LS}\left(l_1^n - l_1^{n-1} l_2\right) &= \delta_{S_1 S'}(-1)^{L'_1+l_2+S_1+J'}\left(n[L_1,L',J,J']\right)^{0.5}\times \\ &\times \begin{Bmatrix} L_1 & S & J \\ J' & 1 & L' \end{Bmatrix}\begin{Bmatrix} l_1 & L'_1 & L_1 \\ L' & 1 & l_2 \end{Bmatrix}\left(l_1^n \alpha_1 L_1 S_1 \{l_1^{n-1}\alpha'_1 L'_1 S'_1\}\right) P^{(1)}_{l_1 l_2}. \end{aligned} \tag{7.3}$$

In this study, we do not have more than two open shells, the acute symbol is used for the core quantum numbers, the δ-function expresses the selection rule of nonchangeable spin momentum, and the radial integral $P^{(1)}_{l_1 l_2}$ is defined by the matrix element of the radial wavefunctions of participating shells:

$$P^{(1)}_{l_1 l_2} = \delta_{l_2, l_1 \pm 1}(-1)^{l_1+\max(l_1,l_2)}\sqrt{\max(l_1,l_2)}\int_0^\infty P_{n_1 l_1} r P_{n_2 l_2} dr. \tag{7.4}$$

Electric dipole transitions can occur only when the oscillator strength (and, correspondently, the line strength) in (7.1) is non-zero. From the properties of the matrix element in the definition of the line strength *S*, it follows that a transition can occur only when the participating states have opposite parity, and $\Delta J = J - J' = 0, \pm 1$. The transition $J = J' = 0$ is not allowed.

In calculating the EUV radiation from tin or xenon plasma, another difficulty may take

place, such as accounting for the transitions from the inner shells. As reported in recent studies [4], some inner levels of the ions with intermediate and heavy atomic numbers may have energies comparable to the ionization potential, which significantly decreases the accuracy of the HF method. For example, in xenon or tin plasma with major radiating wavelength region of interest near 13 nm, transitions from outer shells $4d^q - 4d^{q-1}5p$ must be considered in combination with the transitions $4d^q - 4d^{q-1}4f$ and the transitions from the inner shells, such as $4p^6 4d^q - 4p^5 4d^{q+1}$.

The existence of semi-empirical or experimental information on atomic energy levels may greatly help in improving the accuracy of the ab initio simulation. Unfortunately, such information for the intermediate and high-Z elements, especially their highly excited ions, is not fully presented in the literature [26]. For example, no Sn experimental data are available for the EUV region, except the work of Azarov and Joshi [23], which is not actually dedicated to the 13.5 nm range and only deals with the ion Sn VIII and its transition $4d^7 - 4d^6 5p^1$. According to them, the transition has a very wide range of splitting (near 6 nm), with the major lines being concentrated around 22-23 nm (left figure in Fig. 5). As shown by the right figure in Fig. 5, results of our calculation show very good agreement in shape, width, and place of the transition.

Figure 6 presents the results of our calculation of the EUV transitions for six tin ions, from Sn VIII to Sn XIII. Details of these calculations are presented in Appendix C, and the summary is shown in Table 10.

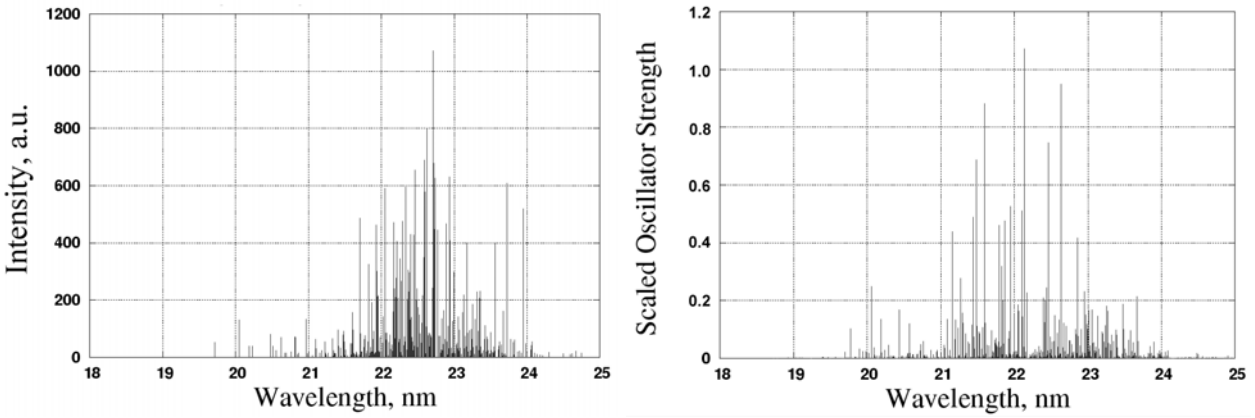

V.I. Azarov and Y.N. Yoshi [23] **HEIGHTS-ATOM calculation**

Fig. 5: Experimental data vs. calculation for Sn VIII $4d^7 - 4d^6 5p^1$ transition

We have determined that the 4*d* - 4*f* and 4*d* - 5*p* transitions only partly cover the EUV range of interest. Among the five ions starting from Sn IX, the highest EUV emission should be from the Sn XI $4d^4 - 4d^3 4f$ transition and from the Sn XII $4d^3 - 4d^2 5p$ transition. Similar results were obtained by means of the Cowan code and are presented in Fig. 7. Despite the difference in the highest values of the oscillator strength, the code also predicts the partial coverage of the EUV range by several transitions, when the highest emission corresponds to the Sn X $4d^5 - 4d^4 4f$ and Sn XI $4d^4 - 4d^3 4f$ transitions.

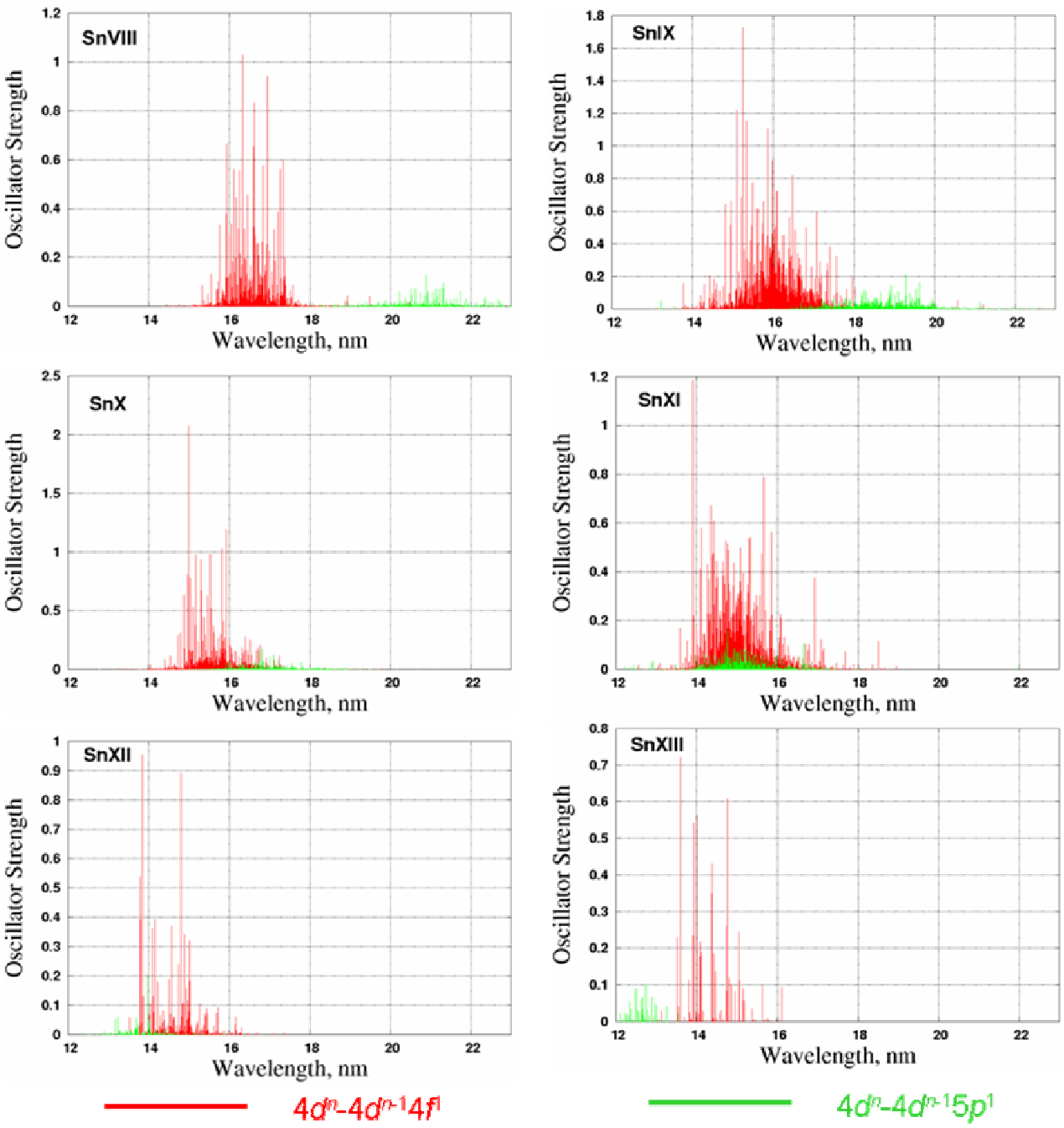

Fig. 6: Calculation of tin EUV transitions by the HEIGHTS-ATOM code

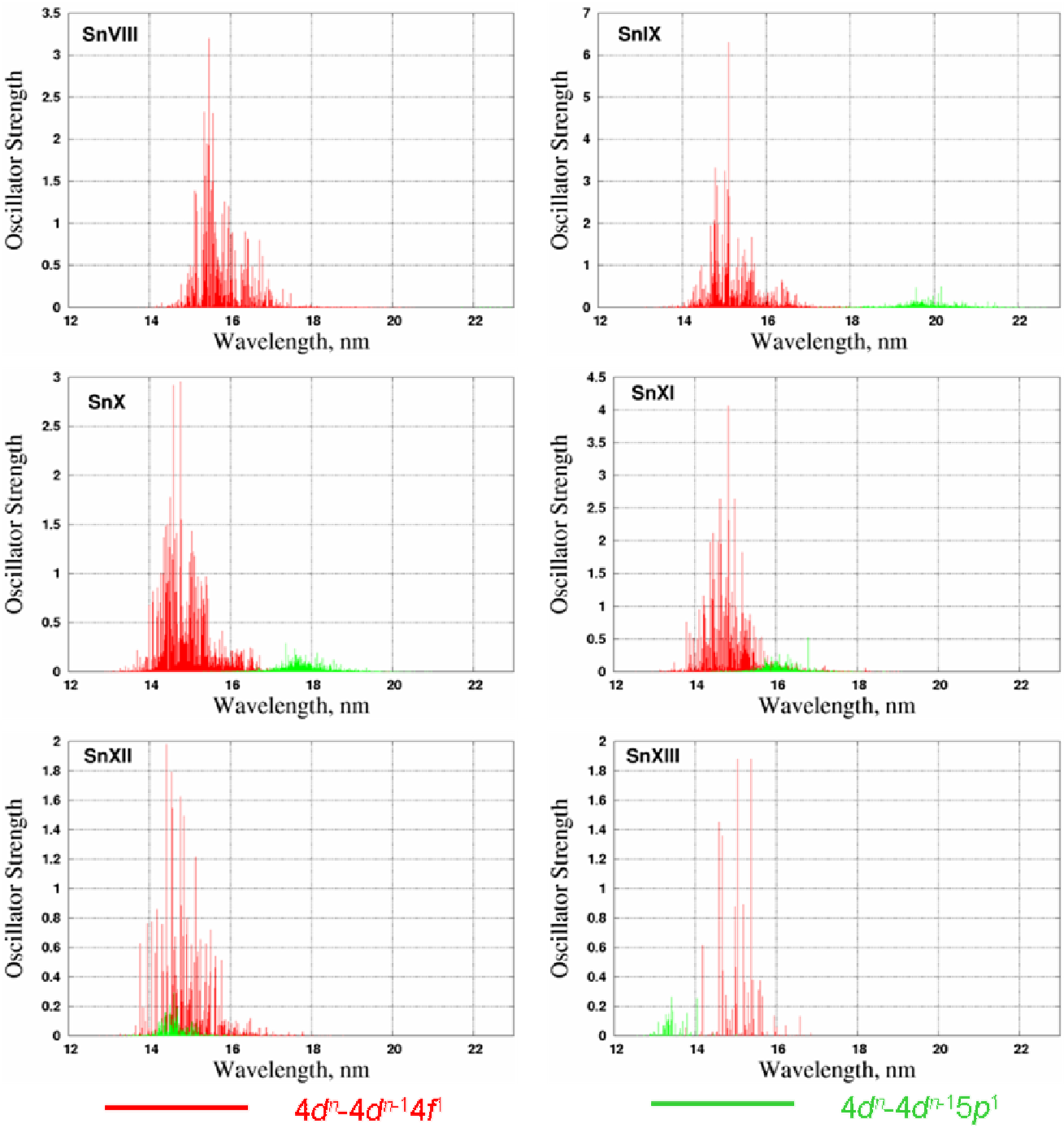

Fig. 7: Calculation of tin EUV transitions by the Cowan code

Table 10: Summary of the tin EUV transitions.

	Sn VIII	Sn IX	Sn X	Sn XI	Sn XII	Sn XIII
Ground Configuration	$4d^7$	$4d^6$	$4d^5$	$4d^4$	$4d^3$	$4d^2$
# levels in GC	19	34	37	34	19	9
Excited 4f Configuration	$4d^64f^1$	$4d^54f^1$	$4d^44f^1$	$4d^34f^1$	$4d^24f^1$	$4d^14f^1$
# levels in 4f EC	346	416	346	206	81	20
Transition array	$4d^7$-$4d^64f^1$	$4d^6$-$4d^54f^1$	$4d^5$-$4d^44f^1$	$4d^4$-$4d^34f^1$	$4d^3$-$4d^24f^1$	$4d^2$-$4d^14f^1$
Total oscillator strength	6.89	5.89	4.80	3.72	2.69	1.72
Splitting, nm	14.204-22.869	12.400-23.859	12.501-22.036	11.963-20.205	12.770-18.238	13.029-16.116
Total transitions	2326	4521	4527	2391	590	62
EUV transitions	0	15	63	101	41	5
Excited 5p Configuration	$4d^65p^1$	$4d^55p^1$	$4d^45p^1$	$4d^35p^1$	$4d^25p^1$	$4d^15p^1$
# levels in 5p EC	180	214	180	110	45	12
Transition array	$4d^7$-$4d^65p^1$	$4d^6$-$4d^55p^1$	$4d^5$-$4d^45p^1$	$4d^4$-$4d^35p^1$	$4d^3$-$4d^25p^1$	$4d^2$-$4d^15p^1$
Total oscillator strength	0.80	0.69	0.58	0.46	0.35	0.23
Splitting, nm	15.580-27.152	12.506-46.903	11.661-22.335	11.644-25.673	11.675-16.077	11.915-13.527
Total transitions	1456	2971	2759	1571	388	46
EUV transitions	0	0	2	66	104	3

8. DETAILED TIN EUV OPACITIES

As discussed in Section 4, the optical emission and absorption coefficients are calculated within the CRE model with line splitting. This model is based on the Hartree-Fock-Slater (HFS) method with both electrostatic and spin-orbit splitting of configurations and spectral lines. Instead of the Racah theory of angular moments for splitting the HFS configuration average energies into levels, we use the better approximation for the split energy levels instead, obtained by the relaxed core Hartree-Fock method in intermediate coupling. In this way, the HFS data for the EUV ions, configurations and transitions are removed, and substituted the improved data directly in the CRE. This guarantees that the EUV range will be covered only by those transitions that we have calculated accurately by the HF method, while the other energy ranges will still be calculated as previously. The size of the generated EUV optical tables is not very large (around 20-40 MB of disk space) due to the very narrow energy range and relatively small number of transitions within that range. Therefore, it is unnecessary to provide additional modifications of the result tables, such as group averaging, as we did previously to reduce the number of spectral points and the amount of required disk space.

In Fig. 8 we present results of our computation of the Sn emission and absorption coefficients in the EUV range of 13.23-13.77 nm or 90.04-93.71 eV, for the typical EUV temperature and density ranges, such as 10-30 eV and 10^{16}-10^{19} cm^{-3}. The coefficients are very dense, when density is around 10^{17} cm^{-3}, and become sparse when the density is higher (up to 10^{19} cm^{-3}) or lower (below 10^{16} cm^{-3}). The results of this calculation indicate that, to maximize the EUV output, the EUV source needs to operate within the named density range.

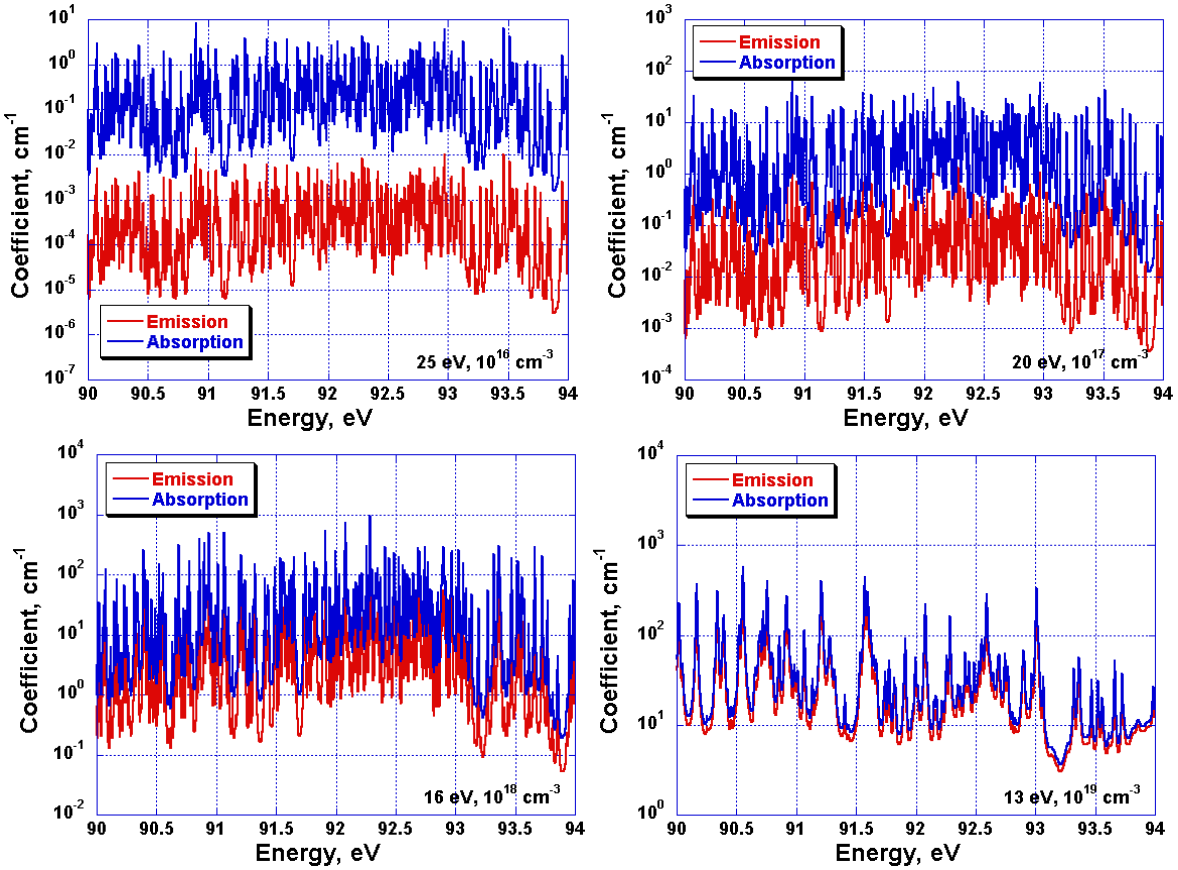

Fig. 8: Tin plasma optical coefficients in the EUV range

CONCLUSION

The report reviewed the major atomic and plasma methods we use within the comprehensive HEIGHTS-EUV package. The methods differ in accuracy, completeness, and complication. The ion states, populations of atomic levels, and optical coefficients, such as emission and absorption coefficients, are calculated by means of the combination of the HFS atomic model and CRE plasma model with splitting atomic levels. The accuracy of these methods is satisfactory to simulate the plasma magnetohydrodynamic behavior, but insufficient to generate the plasma spectroscopic characteristics. Significant accuracy improvement is achieved by using the advanced LSD HF in intermediate coupling atomic method. However, empirical correction of atomic energy levels is necessary to obtain the spectroscopic accuracy of the data and meet the 2% bandwidth requirement of leading EUV source manufacturers within the 13.5 nm range. The applicability of the methods is demonstrated for the tin ions and plasma. Detail atomic and plasma properties, such as energy levels, oscillator strengths, equation of state, relative ion concentrations, wide range opacities, and EUV range opacities near 13.5 nm are calculated, and compared with the available experimental results. The presented results are used by the authors in simulation the dynamics and characteristics of various EUV sources.

ACKNOWLEDGMENTS

The major part of this work is supported by the International SEMATECH and Intel Corp.

REFERENCES

1. Peter J. Silverman, "The Intel Lithography Roadmap," Intel Technology Journal, **6** (2), 55 (2002).
2. V. Bakshi, "Welcome and Introduction," EUV Source Workshop, Santa Clara, CA, Feb. 22, 2004.
3. A. Hassanein, V. Sizyuk, V. Tolkach, V. Morozov, and B. Rice, "HEIGHTS Initial Simulation of Discharge Produced Plasma Hydrodynamics and Radiation Transport for EUV Lithography," presented at the 28th SPIE Annual International Symposium and Education Program on Microlithography, Santa Clara, CA, February 23-28, 2003, Proc. of SPIE, Vol. 5037, 714-727.
4. A. Hassanein, V. Sizyuk, V. Tolkach, V. Morozov, T. Sizyuk, B. Rice, and V. Bakshi, "Simulation and Optimization of DPP Hydrodynamics and Radiation Transport for EUV Lithography Devices," Proc. of SPIE Microlithography 2004 Conference, Santa Clara, CA, Feb. 22-27, 2004, pp. 413-422.
5. V. Tolkach, V. Morozov, and A. Hassanein, "Development of Comprehensive Models for Opacities and Radiation Transport for IFE Systems," ANL Report ANL-ET/02-23 (2002).
6. I. I. Sobelman, *Introduction to the Theory of Atomic Spectra*, Oxford, Pergamon Press (1972).
7. E. U. Condon and G. H. Shortly, *The Theory of Atomic Spectra*, U.K., Cambridge University Press (1964).
8. R. D. Cowan, *The Theory of Atomic Structure and Spectra*, Berkeley, Univ. of California Press (1981).
9. J. C. Slater, Phys. Rev. **81**, 385 (1951).
10. G. Racah, Phys. Rev. **76**, 1352 (1949).
11. G. Racah, Phys. Rev. **85**, 381 (1952).
12. T. Holstein, Phys. Rev. **72**, 1212 (1947).
13. J. P. Apruzese, et al., J. Quant. Spectrosc. Radiat. Transfer, **23**, 479 (1980).
14. J. Pankert et al, Status of Philips Extreme UV Source, unpublished notes.
15. N.N. Kalitkin, *Properties of the Matter and MHD-Programs*, Preprint, M.V. Keldysh Institute of Applied Mathematics, Moscow, 85, 1985 (in Russian).

16. L. Huxley and R. Crompton, *The Diffusion and Drift of Electrons in Gases*, Woodhouse, NY, Wiley (1974).

17. H. R. Griem, *Spectral Line Broadening by Plasmas*, Academic Press, New York (1974).

18. H. Würz, S. Pestchanyi, I. Landman, B. Bazylev, V. Tolkach, and F. Kappler, Fusion Sci. Technol. **40**, N3, 191 (2001).

19. B. N. Bazylev, V. I. Tolkach, et al., "The Calculation of Optical Properties of Atoms and Ions," Kernforschungzentrum Karlsruhe, Interner Bericht (1994).

20. http://physics. nist.gov.

21. R. D. Cowan and N. J. Peacock, Astrophys. J. **142**, 390 (1965).

22. S.S. Churiliov, Y.N. Yoshi, J. Reader, and R.R. Kildiyarova, "Analysis of the $4p^6 4d^8$ – ($4d^7 5p + 4d^7 4f + 4p^5 4d^9$) Transitions in Xe XI Ion", to be published.

23. V. I. Azarov and Y. N. Joshi, "Analysis of the $4d^7$ - $4d^6$ 5p Transition Array of the Eighth Spectrum of Tin: Sn VIII," J. Phys. B: At. Mol. Opt. Phys. **26**, 3495-3514 (1993).

24. U. Fano and G. Racah, *Irreducible Tensorial Sets*, Academic Press, New York (1959).

25. G. Racah, II, Phys. Rev. **62**, 438 (1942).

26. Ch. E. Moore, "Atomic Energy Levels as Derived from the Analyses of Optical Spectra," U.S. Dept. of Commerce, National Bureau of Standards, Washington, D.C., p.3 (1949).

APPENDIX A

The tables that follow present the Sn VIII – Sn XIII energies of the inner shells, calculated by the HEIGHTS-ATOM relaxed-core LSD HF (for each ground term), and configuration-average energies, calculated by the HEIGHTS-ATOM HFS (HFS), and the Cowan code (CHF). All energies are given in Ry.

Table A 1: Energies of Sn VIII inner shells by various methods.

	$1s^2$	$2s^2$	$2p^6$	$3s^2$	$3p^6$	$3d^{10}$	$4s^2$	$4p^6$	$4d^7$
$^2{}_3P$	2091.31	322.66	298.60	71.54	61.71	45.34	18.70	15.06	10.26
$^4{}_3P$	2091.30	322.65	298.60	71.54	61.70	45.34	18.69	15.05	10.28
$^2{}_1D$	2091.33	322.68	298.62	71.56	61.73	45.36	18.71	15.07	10.17
$^2{}_3D$	2091.31	322.66	298.61	71.54	61.71	45.35	18.70	15.06	10.23
$^2{}_3F$	2091.32	322.67	298.61	71.55	61.72	45.35	18.70	15.06	10.21
$^4{}_3F$	2091.29	322.64	298.59	71.53	61.69	45.33	18.69	15.05	10.33
$^2{}_3G$	2091.30	322.65	298.60	71.54	61.70	45.34	18.70	15.05	10.28
$^2{}_3H$	2091.31	322.66	298.60	71.54	61.71	45.34	18.70	15.06	10.26
HFS	2156.88	336.92	309.29	73.29	63.48	46.52	18.93	15.71	10.39
CHF	2165.78	341.10	307.07	75.36	63.88	46.07	19.49	15.70	10.16

Table A 2: Energies of Sn IX inner shells by various methods.

	$1s^2$	$2s^2$	$2p^6$	$3s^2$	$3p^6$	$3d^{10}$	$4s^2$	$4p^6$	$4d^6$
$^1{}_0S$	2093.31	324.67	300.62	73.48	63.65	47.29	20.39	16.69	11.65
$^1{}_4S$	2093.28	324.64	300.59	73.45	63.62	47.26	20.37	16.68	11.81
$^3{}_2P$	2093.27	324.63	300.58	73.45	63.62	47.26	20.37	16.68	11.85
$^3{}_4P$	2093.26	324.63	300.57	73.44	63.61	47.25	20.37	16.67	11.88
$^1{}_2D$	2093.29	324.65	300.60	73.47	63.64	47.27	20.38	16.69	11.73
$^1{}_4D$	2093.27	324.64	300.58	73.45	63.62	47.26	20.37	16.68	11.83
$^3{}_4D$	2093.26	324.62	300.57	73.44	63.61	47.25	20.37	16.67	11.89
$^5{}_4D$	2093.24	324.60	300.55	73.42	63.59	47.23	20.36	16.66	12.02
$^1{}_4F$	2093.27	324.63	300.58	73.45	63.62	47.26	20.37	16.68	11.84
$^3{}_2F$	2093.27	324.64	300.58	73.45	63.62	47.26	20.37	16.68	11.83
$^3{}_4F$	2093.26	324.62	300.57	73.44	63.61	47.25	20.37	16.67	11.90
$^1{}_2G$	2093.28	324.64	300.59	73.46	63.62	47.26	20.38	16.68	11.81
$^1{}_4G$	2093.27	324.63	300.58	73.45	63.62	47.26	20.37	16.68	11.85
$^3{}_4G$	2093.26	324.62	300.57	73.44	63.61	47.25	20.37	16.67	11.92
$^3{}_4H$	2093.26	324.62	300.56	73.44	63.60	47.24	20.36	16.67	11.94
$^1{}_4I$	2093.26	324.62	300.57	73.44	63.61	47.25	20.37	16.67	11.90
HFS	2158.91	338.97	311.34	75.26	65.45	48.50	20.69	17.44	12.04
CHF	2167.73	343.06	309.04	77.26	65.78	47.97	21.17	17.33	11.78

Table A 3: Energies of Sn X inner shells by various methods.

	$1s^2$	$2s^2$	$2p^6$	$3s^2$	$3p^6$	$3d^{10}$	$4s^2$	$4p^6$	$4d^5$
$^{2}_{5}S$	2095.33	326.70	302.65	75.44	65.61	49.25	22.10	18.35	13.52
$^{6}_{5}S$	2095.28	326.66	302.61	75.40	65.57	49.21	22.08	18.33	13.84
$^{2}_{3}P$	2095.35	326.72	302.67	75.46	65.63	49.27	22.11	18.36	13.36
$^{4}_{3}P$	2095.31	326.68	302.63	75.42	65.59	49.23	22.09	18.34	13.66
$^{2}_{1}D$	2095.35	326.72	302.67	75.46	65.63	49.27	22.11	18.36	13.38
$^{2}_{3}D$	2095.33	326.71	302.66	75.45	65.61	49.25	22.10	18.35	13.48
$^{2}_{5}D$	2095.33	326.70	302.65	75.44	65.61	49.25	22.10	18.35	13.53
$^{4}_{5}D$	2095.31	326.68	302.63	75.43	65.59	49.23	22.09	18.34	13.65
$^{2}_{3}F$	2095.32	326.69	302.64	75.43	65.60	49.24	22.09	18.35	13.58
$^{2}_{5}F$	2095.33	326.70	302.65	75.44	65.61	49.25	22.10	18.35	13.55
$^{4}_{3}F$	2095.32	326.69	302.64	75.43	65.60	49.24	22.09	18.35	13.59
$^{2}_{3}G$	2095.34	326.71	302.66	75.45	65.62	49.26	22.10	18.35	13.45
$^{2}_{5}G$	2095.32	326.69	302.64	75.44	65.60	49.24	22.10	18.35	13.57
$^{4}_{5}G$	2095.31	326.68	302.63	75.42	65.59	49.23	22.09	18.34	13.69
$^{2}_{3}H$	2095.32	326.69	302.64	75.44	65.60	49.24	22.10	18.35	13.57
$^{2}_{5}I$	2095.32	326.69	302.64	75.43	65.60	49.24	22.09	18.34	13.62
HFS	2161.04	341.11	313.49	77.32	67.51	50.57	22.50	19.22	13.75
CHF	2169.78	345.13	311.10	79.25	67.77	49.96	22.91	19.01	13.46

Table A 4: Energies of Sn XI inner shells by various methods.

	$1s^2$	$2s^2$	$2p^6$	$3s^2$	$3p^6$	$3d^{10}$	$4s^2$	$4p^6$	$4d^4$
$^{1}_{0}S$	2097.52	328.90	304.85	77.54	67.71	51.36	23.90	20.09	14.93
$^{1}_{4}S$	2097.49	328.87	304.82	77.52	67.69	51.33	23.88	20.08	15.19
$^{3}_{2}P$	2097.49	328.87	304.82	77.51	67.69	51.33	23.88	20.07	15.25
$^{3}_{4}P$	2097.48	328.86	304.81	77.51	67.68	51.32	23.88	20.07	15.30
$^{1}_{2}D$	2097.51	328.89	304.84	77.53	67.70	51.34	23.89	20.08	15.06
$^{1}_{4}D$	2097.49	328.87	304.82	77.52	67.69	51.33	23.88	20.08	15.21
$^{3}_{4}D$	2097.48	328.86	304.81	77.51	67.68	51.32	23.88	20.07	15.32
$^{5}_{4}D$	2097.46	328.84	304.79	77.49	67.66	51.30	23.86	20.06	15.52
$^{1}_{4}F$	2097.49	328.87	304.82	77.52	67.69	51.33	23.88	20.08	15.23
$^{3}_{2}F$	2097.49	328.87	304.82	77.52	67.69	51.33	23.88	20.08	15.22
$^{3}_{4}F$	2097.48	328.86	304.81	77.51	67.68	51.32	23.87	20.07	15.34
$^{1}_{2}G$	2097.49	328.87	304.82	77.52	67.69	51.33	23.88	20.08	15.19
$^{1}_{4}G$	2097.49	328.87	304.82	77.51	67.68	51.33	23.88	20.07	15.26
$^{3}_{4}G$	2097.47	328.86	304.81	77.50	67.68	51.32	23.87	20.07	15.36
$^{3}_{4}H$	2097.47	328.85	304.80	77.50	67.67	51.32	23.87	20.07	15.39
$^{1}_{4}I$	2097.48	328.86	304.81	77.51	67.68	51.32	23.88	20.07	15.33
HFS	2163.27	343.36	315.74	79.46	69.65	52.73	24.37	21.06	15.52
CHF	2171.93	347.29	313.27	81.32	69.85	52.04	24.71	20.74	15.20

Table A 5: Energies of Sn XII inner shells by various methods.

	$1s^2$	$2s^2$	$2p^6$	$3s^2$	$3p^6$	$3d^{10}$	$4s^2$	$4p^6$	$4d^3$
$^2{}_3P$	2099.73	331.12	307.07	79.66	69.84	53.48	25.71	21.85	17.11
$^4{}_3P$	2099.73	331.12	307.07	79.66	69.83	53.48	25.70	21.85	17.17
$^2{}_1D$	2099.75	331.14	307.09	79.68	69.85	53.50	25.72	21.86	16.86
$^2{}_3D$	2099.74	331.13	307.08	79.67	69.84	53.49	25.71	21.85	17.04
$^2{}_3F$	2099.74	331.13	307.08	79.67	69.85	53.49	25.71	21.85	16.98
$^4{}_3F$	2099.72	331.11	307.06	79.65	69.83	53.47	25.70	21.84	17.30
$^2{}_3G$	2099.73	331.12	307.07	79.66	69.83	53.48	25.71	21.85	17.16
$^2{}_3H$	2099.73	331.12	307.07	79.66	69.84	53.48	25.71	21.85	17.11
HFS	2165.59	345.70	318.08	81.68	71.88	54.97	26.29	22.95	17.34
CHF	2174.18	349.55	315.53	83.48	72.01	54.20	26.56	22.53	16.99

Table A 6: Energies of Sn XIII inner shells by various methods.

	$1s^2$	$2s^2$	$2p^6$	$3s^2$	$3p^6$	$3d^{10}$	$4s^2$	$4p^6$	$4d^2$
$^1{}_0S$	2102.11	333.50	309.46	81.92	72.10	55.75	27.60	23.68	18.42
$^3{}_2P$	2102.09	333.48	309.43	81.90	72.08	55.73	27.59	23.67	18.91
$^1{}_2D$	2102.08	333.48	309.43	81.90	72.08	55.73	27.59	23.67	18.93
$^3{}_2F$	2102.08	333.47	309.43	81.89	72.07	55.72	27.59	23.67	19.11
$^1{}_2G$	2102.09	333.48	309.44	81.90	72.08	55.73	27.59	23.68	18.84
HFS	2168.01	348.13	320.52	83.99	74.19	57.30	28.26	24.89	19.21
CHF	2176.53	351.91	317.88	85.72	74.24	56.44	28.46	24.37	18.84

APPENDIX B

Table B 1: Calculation of Excited Sn VIII $4d^6\ 5p^1$ Energy Levels for J = 0.5 to 7.5.

	Exp, cm^{-1}	HEIGHTS-ATOM (th)		HEIGHTS-ATOM (fit)	
		Energy, cm^{-1}	Acc	Energy, cm^{-1}	Acc
J = 0.5		583884		573525	
		562919		519206	
		541185		512028	
	500368	534418	6.80%	504989	0.92%
		523367		498885	
	489629	519742	6.15%	498284	1.77%
	488019	517840	6.11%	494478	1.32%
		512587		492732	
	481842	509309	5.70%	480701	0.24%
	477108	504634	5.77%	473882	0.68%
	472126	500117	5.93%	467242	1.03%
	471218	498509	5.79%	464876	1.35%
	465949	495311	6.30%	464272	0.36%
	461577	494611	7.16%	463868	0.50%
	460713	493444	7.10%	462081	0.30%
	454426	490821	8.01%	459414	1.10%
		478692		447917	
	447257	467664	4.56%	438583	1.94%
	440723	454082	3.03%	428189	2.84%
		442601		415719	
		333018		397768	
J = 1.5		631480		577523	
	534686	576684	7.85%	525889	1.65%
	519436	546492	5.21%	512905	1.26%
		539107		509584	
		535729		507719	
	504724	525654	4.15%	504462	0.05%
	501631	519677		502082	
	499959	516906		500127	
	496028	511132	3.05%	495191	0.17%
	495030	509260	2.87%	494291	0.15%
	491031	507777	3.41%	490895	0.03%
	487686	506419	3.84%	490597	0.60%
	486754	506006	3.96%	486514	0.05%
	480979	502776	4.53%	483837	0.59%
	477124	499717	4.74%	480523	0.71%
	476998	498653	4.54%	476597	0.08%
	475226	494391	4.03%	468894	1.33%
	473695	493731	4.23%	468424	1.11%
	472802	492453	4.16%	466912	1.25%
	471728	488591	3.57%	463961	1.65%
	468196	487621	4.15%	463037	1.10%
	467855	486471	3.98%	462116	1.23%
	466132	485388	4.13%	461733	0.94%
	462285	484004	4.70%	459771	0.54%
	460754	481977	4.61%	459183	0.34%
	458086	480948	4.99%	457751	0.07%
	453056	477237	5.34%	456223	0.70%
	450221	475461	5.61%	452745	0.56%
	446745	467179	4.57%	446135	0.14%

	Exp, cm^{-1}	HEIGHTS-ATOM (th)		HEIGHTS-ATOM (fit)	
		Energy, cm^{-1}	Acc	Energy, cm^{-1}	Acc
J = 1.5	445440	461389	3.58%	438412	1.58%
		456199		432339	
	440430	453472	2.96%	430069	2.35%
		451651		424911	
		439160		416616	
		428142		407587	
J = 2.5	533165	557935	4.65%	526538	1.24%
	523450	547626	4.62%	514874	1.64%
	512335	536816	4.78%	512414	0.02%
		527495		508299	
		523083		504102	
	505728	519536	2.73%	503210	0.50%
	504726	518953	2.82%	498045	1.32%
	500691	516106	3.08%	496104	0.92%
	498841	515045	3.25%	494151	0.94%
	492383	513207	4.23%	493709	0.27%
	490580	510393	4.04%	493641	0.62%
	489111	510090	4.29%	491059	0.40%
	486321	507815	4.42%	489120	0.58%
	485655	506014	4.19%	483547	0.43%
	480770	505838	5.21%	482445	0.35%
	478920	502632	4.95%	480369	0.30%
	476748	499066	4.68%	476790	0.01%
	475671	497944	4.68%	475127	0.11%
	474586	497657	4.86%	471899	0.57%
	473497	494637	4.46%	470811	0.57%
	469860	492985	4.92%	468674	0.25%
	469163	492757	5.03%	467824	0.29%
		491815		464874	
	464919	488818	5.14%	464416	0.11%
	464306	488424	5.19%	464265	0.01%
	463037	487686	5.32%	463018	0.00%
	461128	487561	5.73%	461681	0.12%
	458480	483930	5.55%	460279	0.39%
	456344	482526	5.74%	460051	0.81%
	455525	481231	5.64%	459430	0.86%
	448522	478266	6.63%	458353	2.19%
	446993	477250	6.77%	455867	1.99%
	446190	472860	5.98%	450700	1.01%
	443018	460608	3.97%	436808	1.40%
	442762	454023	2.54%	430444	2.78%
	438874	451703	2.92%	429691	2.09%
	437418	445556	1.86%	423489	3.18%
	424491	437722	3.12%	417074	1.75%
		427930		407807	
J = 3.5		557597		526611	
	518072	549816	6.13%	524211	1.19%
		526374		515604	
	508910	522933	2.76%	507783	0.22%
	504960	520877	3.15%	500794	0.83%

	Exp, cm^{-1}	HEIGHTS-ATOM (th)		HEIGHTS-ATOM (fit)	
		Energy, cm^{-1}	Acc	Energy, cm^{-1}	Acc
J = 3.5	503073	515913	2.55%	497733	1.06%
	500095	514990	2.98%	496876	0.64%
	493417	512400	3.85%	493332	0.02%
	490476	511958	4.38%	491506	0.21%
	489608	508802	3.92%	491394	0.36%
	483311	508519	5.22%	488191	1.01%
	482684	508047	5.25%	487167	0.93%
	479577	506247	5.56%	482413	0.59%
	478651	498960	4.24%	480729	0.43%
	475560	498207	4.76%	476618	0.22%
	474209	496793	4.76%	475006	0.17%
	473750	493543	4.18%	474712	0.20%
	471667	491814	4.27%	473714	0.43%
	468623	489998	4.56%	469676	0.22%
	467779	489575	4.66%	467527	0.05%
		489453		466294	
	465835	486953	4.53%	465443	0.08%
	463394	485124	4.69%	464932	0.33%
	460431	481234	4.52%	463931	0.76%
	458116	480283	4.84%	461586	0.76%
	456976	480180	5.08%	460426	0.76%
	455804	479593	5.22%	459888	0.90%
	453522	478435	5.49%	459298	1.27%
	450287	475619	5.63%	458111	1.74%
	446786	473761	6.04%	458075	2.53%
	441914	470997	6.58%	457066	3.43%
	440431	451147	2.43%	429032	2.59%
	435896	447785	2.73%	427582	1.91%
	433539	444594	2.55%	420610	2.98%
	424441	437881	3.17%	416643	1.84%
		425746		406908	
J = 4.5	515107	540772	4.98%	528461	2.59%
	507162	522380	3.00%	523207	3.16%
		518564		499472	
		516928		496012	
	490948	511261	4.14%	495353	0.90%
	486066	510653	5.06%	493250	1.48%
	483198	510469	5.64%	486598	0.70%
	479703	502064	4.66%	484400	0.98%
	478116	498494	4.26%	483725	1.17%

	Exp, cm^{-1}	HEIGHTS-ATOM (th)		HEIGHTS-ATOM (fit)	
		Energy, cm^{-1}	Acc	Energy, cm^{-1}	Acc
J = 4.5	475592	494905	4.06%	482304	1.41%
	475027	492628	3.71%	475159	0.03%
	496026	489716	1.27%	471724	4.90%
	468801	487677	4.03%	469423	0.13%
	466888	484774	3.83%	467845	0.21%
	465266	484395	4.11%	466120	0.18%
	462784	481971	4.15%	465145	0.51%
	458604	480468	4.77%	464711	1.33%
	465015	477906	2.77%	462827	0.47%
	455636	476373	4.55%	462236	1.45%
	453389	476057	5.00%	460635	1.60%
	449690	472836	5.15%	460594	2.42%
	445212	468631	5.26%	459643	3.24%
		453068		453318	
	437428	448705	2.58%	426152	2.58%
	429008	439241	2.39%	416550	2.90%
		417250		404998	
J = 5.5		528197		525273	
		515269		494389	
		510292		492923	
	480248	495052	3.08%	492158	2.48%
	473754	493545	4.18%	488672	3.15%
	470673	491572	4.44%	481519	2.30%
	467078	489253	4.75%	470939	0.83%
	465511	482078	3.56%	466755	0.27%
	462536	480252	3.83%	465206	0.58%
	458947	477950	4.14%	464518	1.21%
	456734	472273	3.40%	462895	1.35%
	454027	471168	3.78%	461733	1.70%
	445145	469840	5.55%	460613	3.47%
	443110	454030	2.46%	454017	2.46%
		442707		416770	
J = 6.5	480421	497796	3.62%	495274	3.09%
	468370	489374	4.48%	487697	4.13%
	462580	480100	3.79%	465563	0.64%
		473009		464119	
	457182	470849	2.99%	461623	0.97%
		460326		460824	
7.5		495689		490111	
		472619		463285	

APPENDIX C

The tables that follow include the Sn IX – Sn XIII EUV transitions in the 13.5 ± 2 % nm bandwidth (13.23-13.77 nm). The energy of a transition is calculated as difference of total energies of the excited level *i* and the ground level *j*. Columns 1 and 2 contain the total energies, column 3 shows the total moments of the source and target levels, column 5 contains the transition wavelength, and the last column contains non-dimensional oscillator strength.

Table C 1: Calculation of Sn IX $4d^6$-$4d^5 4f^1$ EUV transitions.

Lower level, Ry	Upper level, Ry	$J_i - J_j$	Energy, Ry	λ, nm	f_{ij}
12269.71	12276.62	1-2	6.902232	13.20231	0.000104
12269.27	12276.10	1-2	6.830029	13.34188	0.000018
12269.93	12276.68	4-4	6.752693	13.49468	0.000424
12269.27	12276.00	1-2	6.736535	13.52705	0.000107
12269.68	12276.39	3-4	6.715597	13.56922	0.000879
12269.93	12276.64	4-3	6.710891	13.57874	0.006395
12269.98	12276.68	5-4	6.700022	13.60076	0.000076
12269.70	12276.39	3-4	6.693687	13.61364	0.000300
12269.27	12275.96	1-2	6.692024	13.61702	0.000057
12270.01	12276.68	5-4	6.676483	13.64872	0.000121
12270.03	12276.68	3-4	6.650419	13.70221	0.001019
12269.98	12276.62	1-2	6.640434	13.72281	0.000015
12270.00	12276.64	2-3	6.635490	13.73304	0.003664
12269.68	12276.31	3-3	6.629072	13.74633	0.009445
12269.68	12276.30	3-4	6.623991	13.75688	0.000517
12269.68	12276.30	3-2	6.618909	13.76744	0.155425
12270.00	12276.62	2-2	6.612253	13.78130	0.005178

Table C 2: Calculation of Sn X $4d^5$-$4d^4 4f^1$ EUV transitions.

Lower level, Ry	Upper level, Ry	$J_i - J_j$	Energy, Ry	λ, nm	f_{ij}
12258.02	12264.91	2.5-3.5	6.891484	13.22290	0.000090
12258.42	12265.31	3.5-2.5	6.882666	13.23984	0.000008
12258.03	12264.91	4.5-3.5	6.880646	13.24373	0.006416
12258.03	12264.90	4.5-5.5	6.875768	13.25313	0.000021
12258.03	12264.90	4.5-4.5	6.870598	13.26310	0.002518
12258.44	12265.31	1.5-2.5	6.865376	13.27319	0.000001
12258.02	12264.88	2.5-2.5	6.861611	13.28047	0.000428
12258.02	12264.87	2.5-1.5	6.853315	13.29655	0.000071
12258.46	12265.31	2.5-2.5	6.843287	13.31603	0.000005
12258.46	12265.31	1.5-2.5	6.841684	13.31915	0.000002
12258.50	12265.31	3.5-2.5	6.808647	13.38378	0.000005
12258.02	12264.81	2.5-3.5	6.797375	13.40597	0.000138
12258.51	12265.31	2.5-2.5	6.795462	13.40975	0.000001
12258.03	12264.81	4.5-3.5	6.786537	13.42738	0.003027
12258.52	12265.31	1.5-2.5	6.782472	13.43543	0.000008
12258.52	12265.31	3.5-2.5	6.781388	13.43758	0.000010
12258.15	12264.92	2.5-2.5	6.771324	13.45755	0.000122
12258.16	12264.92	3.5-2.5	6.769100	13.46197	0.000056
12258.54	12265.31	1.5-2.5	6.765783	13.46857	0.000002
12258.16	12264.92	1.5-2.5	6.759534	13.48102	0.000465
12258.17	12264.92	2.5-2.5	6.755462	13.48915	0.000001
12258.15	12264.91	2.5-3.5	6.755014	13.49004	0.000152
12258.16	12264.91	3.5-3.5	6.752790	13.49448	0.000054
12258.02	12264.76	2.5-1.5	6.745445	13.50918	0.000561
12258.17	12264.91	2.5-3.5	6.739152	13.52179	0.000011
12258.15	12264.88	2.5-2.5	6.725141	13.54996	0.000044
12258.16	12264.88	3.5-2.5	6.722917	13.55445	0.000068
12258.58	12265.31	2.5-2.5	6.722120	13.55605	0.000013
12258.58	12265.31	3.5-2.5	6.720895	13.55852	0.000004
12258.15	12264.87	2.5-1.5	6.716845	13.56670	0.000029
12258.16	12264.88	1.5-2.5	6.713351	13.57376	0.000063

12258.03	12264.74	4.5-5.5	6.711484	13.57754	0.000071
12258.17	12264.88	2.5-2.5	6.709279	13.58200	0.000012
12258.16	12264.87	1.5-1.5	6.705055	13.59055	0.000001
12258.61	12265.31	3.5-2.5	6.699278	13.60227	0.000011
12258.61	12265.31	2.5-2.5	6.695434	13.61008	0.000001
12258.61	12265.31	3.5-2.5	6.691390	13.61831	0.000003
12258.63	12265.31	2.5-2.5	6.679497	13.64256	0.000002
12258.63	12265.31	3.5-2.5	6.676075	13.64955	0.000014
12258.63	12265.31	2.5-2.5	6.673786	13.65423	0.000002
12258.25	12264.92	2.5-2.5	6.671947	13.65799	0.000805
12258.64	12265.31	1.5-2.5	6.666580	13.66899	0.000002
12258.15	12264.81	2.5-3.5	6.660905	13.68064	0.000015
12258.65	12265.31	3.5-2.5	6.659999	13.68250	0.000012
12258.65	12265.31	3.5-2.5	6.658693	13.68518	0.000002
12258.16	12264.81	3.5-3.5	6.658681	13.68521	0.000006
12258.27	12264.92	3.5-2.5	6.655962	13.69080	0.000001
12258.25	12264.91	2.5-3.5	6.655637	13.69146	0.000034
12258.02	12264.66	2.5-3.5	6.646327	13.71064	0.000674
12258.17	12264.81	2.5-3.5	6.645043	13.71329	0.000003
12258.28	12264.92	1.5-2.5	6.640648	13.72237	0.000026
12258.27	12264.91	3.5-3.5	6.639652	13.72443	0.000739
12258.03	12264.66	4.5-3.5	6.635489	13.73304	0.001069
12258.29	12264.92	2.5-2.5	6.634390	13.73531	0.000192
12258.03	12264.66	4.5-4.5	6.631867	13.74054	0.000982
12258.68	12265.31	3.5-2.5	6.630319	13.74375	0.000006
12258.25	12264.88	2.5-2.5	6.625764	13.75319	0.000755
12258.30	12264.92	3.5-2.5	6.625658	13.75341	0.000123
12258.30	12264.92	1.5-2.5	6.623227	13.75846	0.000087
12258.68	12265.31	3.5-2.5	6.622783	13.75938	0.000003
12258.69	12265.31	2.5-2.5	6.619029	13.76719	0.000004
12258.69	12265.31	3.5-2.5	6.618500	13.76829	0.000006
12258.29	12264.91	2.5-3.5	6.618080	13.76916	0.000265
12258.02	12264.63	2.5-2.5	6.617922	13.76949	0.001654
12258.25	12264.87	2.5-1.5	6.617468	13.77044	0.000397

Table C 3: Calculation of Sn X $4d^5$-$4d^4 5p^1$ EUV transitions.

Lower level, Ry	Upper level, Ry	$J_i - J_j$	Energy, Ry	λ, nm	f_{ij}
12257.49	12264.43	1.5-2.5	6.940224	13.13004	0.001501
12257.49	12264.34	1.5-1.5	6.847644	13.30756	0.000050
12257.49	12264.32	1.5-2.5	6.825849	13.35005	0.000129
12257.49	12264.09	1.5-1.5	6.596839	13.81350	0.000374

Table C 4: Calculation of Sn XI $4d^4$-$4d^3 4f^1$ EUV transitions.

Lower level, Ry	Upper level, Ry	$J_i - J_j$	Energy, Ry	λ, nm	f_{ij}
12244.80	12251.69	3-4	6.894059	13.21796	0.000055
12244.81	12251.69	3-4	6.883747	13.23776	0.000058
12244.88	12251.76	3-2	6.883176	13.23886	0.000508
12244.81	12251.69	5-4	6.883083	13.23904	0.004176
12244.88	12251.76	2-2	6.882066	13.24100	0.000015
12244.88	12251.76	1-2	6.879515	13.24591	0.003504
12244.91	12251.79	1-1	6.873717	13.25708	0.000053
12244.14	12251.02	1-2	6.873667	13.25718	0.000369
12244.51	12251.39	5-4	6.873604	13.25730	0.001224
12244.47	12251.34	3-2	6.872004	13.26038	0.002656
12244.47	12251.33	3-4	6.864104	13.27565	0.000305
12244.47	12251.33	3-3	6.863995	13.27586	0.000018
12244.83	12251.69	4-4	6.863483	13.27685	0.000253
12244.86	12251.73	2-3	6.863419	13.27697	0.000025
12244.90	12251.76	3-2	6.860414	13.28279	0.000159
12244.47	12251.32	3-2	6.856421	13.29052	0.000599
12244.90	12251.76	1-2	6.855721	13.29188	0.000322
12244.88	12251.73	3-3	6.851211	13.30063	0.001243
12244.88	12251.73	2-3	6.850101	13.30278	0.000491
12244.94	12251.79	2-1	6.848238	13.30640	0.000004
12244.91	12251.76	1-2	6.847593	13.30766	0.001264

12244.92	12251.76	3-2	6.836741	13.32878	0.000025
12244.90	12251.73	3-3	6.828449	13.34497	0.002593
12244.94	12251.76	2-2	6.822114	13.35736	0.001967
12244.51	12251.33	5-4	6.819337	13.36280	0.017153
12244.47	12251.29	3-3	6.818086	13.36525	0.003586
12244.88	12251.69	3-4	6.814937	13.37142	0.000004
12244.69	12251.50	5-4	6.812768	13.37568	0.012189
12244.92	12251.73	3-3	6.804776	13.39139	0.000172
12244.71	12251.50	5-4	6.793209	13.41419	0.000441
12244.94	12251.73	4-3	6.793038	13.41453	0.000032
12244.90	12251.69	3-4	6.792175	13.41624	0.000459
12244.94	12251.73	2-3	6.790149	13.42024	0.000633
12245.00	12251.79	2-1	6.788984	13.42254	0.000334
12244.98	12251.76	3-2	6.784687	13.43104	0.000356
12244.69	12251.47	5-5	6.778569	13.44316	0.015460
12244.92	12251.69	3-4	6.768502	13.46316	0.000071
12244.96	12251.73	4-3	6.764406	13.47131	0.001263
12245.00	12251.76	2-2	6.762860	13.47439	0.000119
12244.47	12251.23	3-2	6.757768	13.48454	0.004950
12244.94	12251.69	4-4	6.756764	13.48655	0.000602
12245.00	12251.76	3-2	6.756106	13.48786	0.000226
12244.98	12251.73	3-3	6.752722	13.49462	0.000097
12244.69	12251.44	5-6	6.751473	13.49712	0.000906
12244.95	12251.69	5-4	6.745791	13.50849	0.003608
12244.99	12251.73	4-3	6.741759	13.51656	0.002842
12245.05	12251.79	2-1	6.73515	13.52983	0.000039
12244.61	12251.34	1-2	6.733177	13.53379	0.000329
12245.00	12251.73	2-3	6.730895	13.53838	0.000024
12244.77	12251.50	3-4	6.728196	13.54381	0.000407
12244.96	12251.69	4-4	6.728132	13.54394	0.000021
12244.70	12251.43	2-3	6.727805	13.54460	0.001737
12245.00	12251.73	3-3	6.724141	13.55198	0.002877
12244.61	12251.32	1-2	6.717594	13.56519	0.000322
12244.98	12251.69	3-4	6.716448	13.56750	0.000117
12245.05	12251.76	1-2	6.710335	13.57986	0.000043

12245.05	12251.76	2-2	6.709026	13.58251	0.000138
12245.05	12251.76	3-2	6.70801	13.58457	0.000025
12244.73	12251.44	7-6	6.707233	13.58614	0.169773
12244.99	12251.69	4-4	6.705485	13.58968	0.002073
12245.02	12251.73	4-3	6.704517	13.59165	0.006088
12244.80	12251.50	3-4	6.703394	13.59392	0.000145
12244.47	12251.17	3-4	6.698364	13.60413	0.004650
12244.69	12251.39	5-4	6.697115	13.60667	0.002026
12244.81	12251.50	3-4	6.693082	13.61487	0.000006
12244.81	12251.50	5-4	6.692418	13.61622	0.001374
12245.00	12251.69	3-4	6.687867	13.62548	0.000134
12245.07	12251.76	2-2	6.685994	13.62930	0.000014
12245.08	12251.76	3-2	6.679984	13.64156	0.000071
12244.71	12251.39	5-4	6.677556	13.64652	0.025702
12245.05	12251.73	2-3	6.677061	13.64753	0.001226
12245.05	12251.73	3-3	6.676045	13.64961	0.000421
12244.83	12251.5	4-4	6.672818	13.65621	0.000005
12245.09	12251.76	1-2	6.672154	13.65757	0.000005
12245.02	12251.69	4-4	6.668243	13.66558	0.003290
12244.47	12251.13	3-2	6.664878	13.67248	0.001852
12245.07	12251.73	2-3	6.654029	13.69477	0.000078
12244.77	12251.43	3-3	6.653639	13.69558	0.002406
12244.51	12251.17	5-4	6.653597	13.69566	0.000612
12245.08	12251.73	4-3	6.652822	13.69726	0.000255
12245.14	12251.79	2-1	6.650296	13.70246	0.000002
12245.08	12251.73	3-3	6.648019	13.70715	0.005865
12244.69	12251.33	5-4	6.642848	13.71782	0.046407
12244.47	12251.11	3-3	6.640605	13.72246	0.015694
12244.70	12251.34	2-2	6.640342	13.72300	0.024252
12244.69	12251.33	5-5	6.639916	13.72388	0.000491
12245.05	12251.69	3-4	6.639771	13.72418	0.002333
12244.83	12251.47	4-5	6.638619	13.72656	0.000071
12245.12	12251.76	3-2	6.636858	13.73020	0.000125
12245.15	12251.79	1-1	6.636624	13.73069	0.000243
12245.06	12251.69	5-4	6.633555	13.73704	0.003798

12244.70	12251.33	2-3	6.632333	13.73957	0.004531
12245.13	12251.76	3-2	6.630589	13.74319	0.000848
12244.80	12251.43	3-3	6.628837	13.74682	0.000008
12245.10	12251.73	4-3	6.626732	13.75118	0.013451
12244.70	12251.32	2-2	6.624759	13.75528	0.014526
12244.88	12251.50	3-4	6.624272	13.75629	0.000004
12245.14	12251.76	2-2	6.624172	13.75650	0.000779
12244.47	12251.09	3-2	6.624058	13.75674	0.117769
12244.71	12251.33	5-4	6.623289	13.75833	0.002178
12244.61	12251.23	1-2	6.618941	13.76737	0.000592
12244.81	12251.43	3-3	6.618525	13.76824	0.002580
12245.08	12251.69	4-4	6.616548	13.77235	0.001870
12244.77	12251.39	3-4	6.612543	13.78069	0.001295

Table C 5: Calculation of Sn XI $4d^4$-$4d^3 5p^1$ EUV transitions.

Lower level, Ry	Upper level, Ry	$J_i - J_j$	Energy, Ry	λ, nm	f_{ij}
12244.87	12251.76	2-2	6.889793	13.22615	0.000571
12244.56	12251.43	3-3	6.868948	13.26628	0.000006
12244.82	12251.69	3-4	6.868550	13.26705	0.000226
12244.86	12251.73	3-3	6.868095	13.26793	0.000245
12244.87	12251.73	2-3	6.857828	13.28780	0.000018
12244.92	12251.76	2-2	6.844043	13.31456	0.000002
12244.86	12251.69	3-4	6.831821	13.33838	0.000156
12244.93	12251.76	2-2	6.829306	13.34329	0.000011
12244.56	12251.39	3-4	6.827852	13.34613	0.001513
12244.94	12251.76	1-2	6.824630	13.35243	0.000002
12244.92	12251.73	2-3	6.812078	13.37704	0.000015
12244.96	12251.76	1-2	6.801678	13.39749	0.000001
12244.93	12251.73	2-3	6.797341	13.40604	0.000109
12244.99	12251.79	2-1	6.795518	13.40964	0.000063
12244.56	12251.34	3-2	6.781485	13.43738	0.000179
12245.01	12251.79	1-1	6.777861	13.44457	0.000008
12244.73	12251.50	4-4	6.773639	13.45295	0.000054

12244.56	12251.33	3-4	6.773585	13.45306	0.000474
12244.56	12251.33	3-3	6.773476	13.45327	0.000496
12244.99	12251.76	2-2	6.769394	13.46138	0.000099
12244.56	12251.32	3-2	6.765902	13.46833	0.000066
12243.96	12250.72	2-2	6.758530	13.48302	0.019647
12245.01	12251.76	3-2	6.752213	13.49564	0.000040
12245.01	12251.76	1-2	6.751737	13.49659	0.000014
12245.04	12251.79	1-1	6.750366	13.49933	0.000020
12245.04	12251.79	2-1	6.749810	13.50044	0.000003
12245.02	12251.76	3-2	6.737754	13.52460	0.000078
12244.99	12251.73	2-3	6.737429	13.52525	0.000068
12244.96	12251.69	5-4	6.733948	13.53224	0.000358
12244.56	12251.29	3-3	6.727567	13.54508	0.000527
12245.00	12251.73	4-3	6.723701	13.55287	0.000042
12245.04	12251.76	2-2	6.723686	13.55290	0.000058
12245.01	12251.73	3-3	6.720248	13.55983	0.000074
12244.98	12251.69	5-4	6.709323	13.58191	0.000016
12245.02	12251.73	3-3	6.705789	13.58907	0.000064
12244.73	12251.43	4-3	6.699082	13.60267	0.000584
12244.65	12251.34	1-2	6.693249	13.61453	0.000273
12245.04	12251.73	2-3	6.691721	13.61764	0.000015
12245.07	12251.76	3-2	6.690117	13.62090	0.000009
12245.00	12251.69	4-4	6.687427	13.62638	0.000306
12245.01	12251.69	3-4	6.683974	13.63342	0.000067
12245.10	12251.79	1-1	6.681993	13.63746	0.000003
12244.82	12251.50	3-4	6.677885	13.64585	0.002136
12244.65	12251.32	1-2	6.677666	13.64630	0.000816
12244.65	12251.32	1-1	6.673463	13.65489	0.000026
12245.02	12251.69	4-4	6.670146	13.66168	0.000014
12245.02	12251.69	3-4	6.669515	13.66298	0.000040
12245.06	12251.73	4-3	6.669084	13.66386	0.000111
12244.56	12251.23	3-2	6.667249	13.66762	0.006923
12245.10	12251.76	3-2	6.660088	13.68231	0.000002
12245.13	12251.79	1-1	6.658900	13.68476	0.000031
12245.07	12251.73	3-3	6.658152	13.68629	0.000093

12244.73	12251.39	4-4	6.657986	13.68663	0.000172
12245.10	12251.76	1-2	6.655869	13.69099	0.000046
12245.12	12251.76	3-2	6.644018	13.71541	0.000252
12244.86	12251.50	3-4	6.641156	13.72132	0.000184
12245.06	12251.69	4-4	6.632810	13.73858	0.000129
12245.13	12251.76	1-2	6.632776	13.73865	0.000036
12245.15	12251.79	2-1	6.631860	13.74055	0.000004
12245.13	12251.76	3-2	6.630311	13.74376	0.000049
12245.10	12251.73	4-3	6.630109	13.74418	0.000310
12245.16	12251.79	1-1	6.629847	13.74472	0.000008
12245.10	12251.73	3-3	6.628123	13.74830	0.000001
12245.13	12251.76	3-2	6.625887	13.75294	0.000002
12245.14	12251.76	3-2	6.625016	13.75475	0.000299
12245.16	12251.79	2-1	6.624865	13.75506	0.000059
12245.07	12251.69	3-4	6.621878	13.76126	0.000045
12245.12	12251.73	3-3	6.612053	13.78171	0.000006

Table C 6: Calculation of Sn XII $4d^3$-$4d^24f^1$ EUV transitions.

Lower level, Ry	Upper level, Ry	$J_i - J_j$	Energy, Ry	λ, nm	f_{ij}
12229.53	12236.42	2.5-3.5	6.893386	13.21925	0.000002
12229.64	12236.52	1.5-1.5	6.872908	13.25864	0.000001
12229.65	12236.52	2.5-1.5	6.872330	13.25976	0.000144
12229.52	12236.37	3.5-4.5	6.857156	13.28910	0.000002
12229.38	12236.22	2.5-3.5	6.835726	13.33076	0.000031
12229.65	12236.47	2.5-2.5	6.826796	13.34820	0.000144
12229.40	12236.22	3.5-3.5	6.819391	13.36269	0.000012
12229.61	12236.42	4.5-3.5	6.816819	13.36773	0.001502
12229.46	12236.28	1.5-1.5	6.815616	13.37009	0.000053
12229.38	12236.19	2.5-2.5	6.811084	13.37899	0.000489
12229.40	12236.21	3.5-4.5	6.808115	13.38482	0.000006
12229.40	12236.19	3.5-2.5	6.794749	13.41115	0.000735
12229.74	12236.52	2.5-1.5	6.776738	13.44680	0.000113
12229.65	12236.42	2.5-3.5	6.776393	13.44748	0.000290

12229.60	12236.37	5.5-4.5	6.772770	13.45467	0.008908
12229.61	12236.37	4.5-4.5	6.767768	13.46462	0.000022
12229.53	12236.28	2.5-1.5	6.747018	13.50603	0.000093
12229.63	12236.37	5.5-4.5	6.740409	13.51927	0.058735
12229.46	12236.19	1.5-2.5	6.733121	13.53390	0.000259
12229.74	12236.47	2.5-2.5	6.731204	13.53776	0.000088
12229.38	12236.10	2.5-1.5	6.715639	13.56914	0.000748
12229.76	12236.47	3.5-2.5	6.712212	13.57606	0.000345
12229.81	12236.52	2.5-1.5	6.702884	13.59496	0.000012
12229.52	12236.22	3.5-3.5	6.701986	13.59678	0.000086
12229.52	12236.21	3.5-4.5	6.690710	13.61969	0.000009
12229.73	12236.42	4.5-3.5	6.689327	13.62251	0.000743
12229.53	12236.22	2.5-3.5	6.689165	13.62284	0.000025
12229.74	12236.42	2.5-3.5	6.680801	13.63989	0.000013
12229.84	12236.52	2.5-1.5	6.677780	13.64606	0.000169
12229.52	12236.19	3.5-2.5	6.677344	13.64696	0.000345
12229.53	12236.19	2.5-2.5	6.664523	13.67321	0.000085
12229.76	12236.42	3.5-3.5	6.661809	13.67878	0.000460
12229.86	12236.52	1.5-1.5	6.660355	13.68177	0.000045
12229.81	12236.47	2.5-2.5	6.657350	13.68794	0.003233
12229.87	12236.52	1.5-1.5	6.646379	13.71054	0.000005
12229.83	12236.47	3.5-2.5	6.637821	13.72821	0.000060
12229.46	12236.10	1.5-1.5	6.637676	13.72851	0.002329
12229.84	12236.47	2.5-2.5	6.632246	13.73975	0.000480
12229.64	12236.28	1.5-1.5	6.630603	13.74316	0.000001
12229.65	12236.28	2.5-1.5	6.630025	13.74436	0.000212
12229.89	12236.52	2.5-1.5	6.629385	13.74568	0.000011
12229.38	12236.00	2.5-2.5	6.621366	13.76233	0.026480
12229.86	12236.47	1.5-2.5	6.614821	13.77595	0.000238

Table C 7: Calculation of Sn XII $4d^3$-$4d^2 5p^1$ EUV transitions.

Lower level, Ry	Upper level, Ry	$J_i - J_j$	Energy, Ry	λ, nm	f_{ij}
12229.21	12236.09	5.5-5.5	6.889494	13.22672	0.058378
12229.34	12236.22	3.5-3.5	6.873589	13.25733	0.008973
12229.65	12236.52	1.5-1.5	6.870590	13.26311	0.000008
12229.55	12236.42	3.5-3.5	6.868564	13.26703	0.000957
12229.65	12236.52	2.5-1.5	6.867963	13.26819	0.002244
12229.21	12236.07	5.5-4.5	6.865747	13.27247	0.016528
12229.51	12236.37	5.5-4.5	6.865665	13.27263	0.003575
12229.56	12236.42	2.5-3.5	6.864338	13.27519	0.000011
12229.34	12236.21	3.5-4.5	6.862313	13.27911	0.010704
12229.24	12236.10	2.5-1.5	6.861139	13.28138	0.000048
12229.14	12236.00	2.5-2.5	6.860717	13.28220	0.009757
12229.57	12236.42	3.5-3.5	6.853586	13.29602	0.000320
12229.57	12236.42	4.5-3.5	6.850612	13.30179	0.000004
12229.43	12236.28	2.5-1.5	6.848516	13.30586	0.000017
12229.16	12236.00	1.5-2.5	6.847643	13.30756	0.000003
12229.63	12236.47	3.5-2.5	6.839352	13.32369	0.001630
12229.38	12236.22	3.5-3.5	6.834203	13.33373	0.000092
12229.24	12236.07	3.5-4.5	6.834143	13.33385	0.006647
12229.37	12236.19	1.5-2.5	6.825507	13.35072	0.000004
12229.65	12236.47	1.5-2.5	6.825056	13.35160	0.000016
12229.69	12236.52	2.5-1.5	6.824887	13.35193	0.000152
12229.38	12236.21	3.5-4.5	6.822927	13.35577	0.000185
12229.65	12236.47	2.5-2.5	6.822429	13.35674	0.001915
12229.46	12236.28	2.5-1.5	6.820155	13.36119	0.000007
12229.55	12236.37	3.5-4.5	6.819513	13.36245	0.003215
12229.66	12236.47	3.5-2.5	6.815752	13.36983	0.003481
12229.28	12236.09	4.5-5.5	6.813038	13.37515	0.000059
12229.57	12236.37	3.5-4.5	6.804535	13.39187	0.000037
12229.57	12236.37	4.5-4.5	6.801561	13.39772	0.000020
12229.72	12236.52	2.5-1.5	6.801304	13.39823	0.000894
12229.47	12236.28	1.5-1.5	6.801297	13.39824	0.000003

12229.48	12236.28	2.5-1.5	6.791484	13.41760	0.000001
12229.43	12236.22	2.5-3.5	6.790663	13.41922	0.000351
12229.28	12236.07	4.5-4.5	6.789291	13.42193	0.003802
12229.63	12236.42	3.5-3.5	6.788949	13.42261	0.006245
12229.14	12235.93	2.5-1.5	6.788017	13.42445	0.003072
12229.43	12236.22	4.5-3.5	6.784212	13.43198	0.016316
12229.69	12236.47	2.5-2.5	6.779353	13.44161	0.000021
12229.74	12236.52	2.5-1.5	6.779084	13.44214	0.002099
12229.70	12236.47	3.5-2.5	6.776985	13.44631	0.008626
12229.16	12235.93	1.5-1.5	6.774943	13.45036	0.000237
12229.65	12236.42	4.5-3.5	6.774473	13.45129	0.001489
12229.43	12236.21	4.5-4.5	6.772936	13.45434	0.002662
12229.65	12236.42	2.5-3.5	6.772026	13.45615	0.000374
12229.14	12235.91	2.5-3.5	6.770873	13.45844	0.006515
12229.75	12236.52	1.5-1.5	6.770853	13.45848	0.000007
12229.24	12236.00	2.5-2.5	6.766866	13.46641	0.000056
12229.24	12236.00	3.5-2.5	6.766419	13.46730	0.009722
12229.43	12236.19	2.5-2.5	6.766021	13.46810	0.000004
12229.66	12236.42	3.5-3.5	6.765349	13.46943	0.002702
12229.14	12235.91	2.5-2.5	6.765115	13.46990	0.007706
12229.46	12236.22	2.5-3.5	6.762302	13.47550	0.008199
12229.51	12236.28	1.5-1.5	6.762258	13.47559	0.000123
12229.72	12236.47	2.5-2.5	6.755770	13.48853	0.000001
12229.16	12235.91	1.5-2.5	6.752041	13.49598	0.000015
12229.53	12236.28	1.5-1.5	6.744460	13.51115	0.000602
12229.63	12236.37	3.5-4.5	6.739898	13.52030	0.009498
12229.46	12236.19	2.5-2.5	6.737660	13.52479	0.000006
12229.48	12236.22	2.5-3.5	6.733631	13.53288	0.000180
12229.74	12236.47	2.5-2.5	6.733550	13.53304	0.001282
12229.37	12236.10	1.5-1.5	6.730062	13.54006	0.000205
12229.69	12236.42	2.5-3.5	6.728950	13.54229	0.000178
12229.34	12236.07	3.5-4.5	6.726953	13.54631	0.012976
12229.70	12236.42	3.5-3.5	6.726582	13.54706	0.000184
12229.65	12236.37	4.5-4.5	6.725422	13.54940	0.012606
12229.75	12236.47	1.5-2.5	6.725319	13.54961	0.000014

12229.70	12236.42	4.5-3.5	6.718144	13.56408	0.018115
12229.56	12236.28	2.5-1.5	6.717970	13.56443	0.000010
12229.66	12236.37	3.5-4.5	6.716298	13.56780	0.003112
12229.48	12236.19	2.5-2.5	6.708989	13.58259	0.000016
12229.72	12236.42	2.5-3.5	6.705367	13.58992	0.004396
12229.51	12236.21	5.5-4.5	6.699219	13.60239	0.000386
12229.78	12236.47	3.5-2.5	6.696956	13.60699	0.000624
12229.24	12235.93	2.5-1.5	6.694166	13.61266	0.000263
12229.38	12236.07	3.5-4.5	6.687567	13.62609	0.000058
12229.74	12236.42	2.5-3.5	6.683147	13.63511	0.001705
12229.70	12236.37	3.5-4.5	6.677531	13.64657	0.004265
12229.24	12235.91	2.5-3.5	6.677022	13.64761	0.000377
12229.24	12235.91	3.5-3.5	6.676575	13.64853	0.021338
12229.24	12235.91	2.5-2.5	6.671264	13.65939	0.000661
12229.24	12235.91	3.5-2.5	6.670817	13.66031	0.010699
12229.43	12236.10	2.5-1.5	6.670576	13.66080	0.000041
12229.70	12236.37	4.5-4.5	6.669093	13.66384	0.001371
12229.55	12236.22	3.5-3.5	6.664343	13.67358	0.021111
12229.53	12236.19	1.5-2.5	6.661965	13.67846	0.000003
12229.43	12236.09	4.5-5.5	6.661323	13.67978	0.003991
12229.86	12236.52	1.5-1.5	6.660873	13.68070	0.000968
12229.56	12236.22	2.5-3.5	6.660117	13.68225	0.005373
12229.34	12236.00	3.5-2.5	6.659229	13.68408	0.001049
12229.55	12236.21	3.5-4.5	6.653067	13.69675	0.055440
12229.57	12236.22	3.5-3.5	6.649365	13.70438	0.020415
12229.78	12236.42	3.5-3.5	6.646553	13.71018	0.000115
12229.57	12236.22	4.5-3.5	6.646391	13.71051	0.000039
12229.46	12236.10	2.5-1.5	6.642215	13.71913	0.000399
12229.55	12236.19	3.5-2.5	6.639701	13.72433	0.000015
12229.57	12236.21	3.5-4.5	6.638089	13.72766	0.033137
12229.43	12236.07	4.5-4.5	6.637576	13.72872	0.034227
12229.37	12236.00	1.5-2.5	6.635789	13.73242	0.001830
12229.56	12236.19	2.5-2.5	6.635475	13.73307	0.000007
12229.57	12236.21	4.5-4.5	6.635115	13.73381	0.008751
12229.28	12235.91	4.5-3.5	6.631723	13.74084	0.000058

12229.65	12236.28	2.5-1.5	6.625658	13.75341	0.000033
12229.57	12236.19	3.5-2.5	6.624723	13.75536	0.000007
12229.47	12236.10	1.5-1.5	6.623357	13.75819	0.000004
12229.38	12236.00	3.5-2.5	6.619843	13.76550	0.000011
12229.58	12236.19	1.5-2.5	6.616343	13.77278	0.000002

Table C 8: Calculation of Sn XIII $4d^2$-$4d^1 4f^1$ EUV transitions.

Lower level, Ry	Upper level, Ry	$J_i - J_j$	Energy, Ry	λ, nm	f_{ij}
12212.30	12219.24	5-4	6.945076	13.12087	0.028954
12212.67	12219.41	3-2	6.740982	13.51812	0.230132
12212.42	12219.14	1-2	6.728113	13.54398	0.040631
12212.30	12219.00	5-4	6.704292	13.59210	0.721355
12212.75	12219.41	2-2	6.658619	13.68533	0.012508
12212.67	12219.32	3-3	6.655111	13.69255	0.007450
12212.80	12219.41	3-2	6.605690	13.79499	0.113100

Table C 9: Calculation of Sn XIII $4d^2$-$4d^1 5p^1$ EUV transitions.

Lower level, Ry	Upper level, Ry	$J_i - J_j$	Energy, Ry	λ, nm	f_{ij}
12212.10	12219.01	2-2	6.912305	13.18307	0.002445
12212.13	12219.01	2-2	6.878340	13.24817	0.041117
12212.27	12219.14	1-2	6.869359	13.26549	0.000677
12212.27	12219.01	1-2	6.736806	13.52650	0.019506

Distribution List for ANL-ET-04/24

Internal:

J. P. Allain	J. N. Brooks	A. Foley
D. Gruen	J. Harmon	A. Hassanein (10)
Z. Insepov	I. Konkashbaev	V. Morozov (5)
J. Norem	R. B. Poeppel	W. Shack
V. A. Sizyuk	S. W. Tam	TIS Files

External:

DOE-SC (5)

ANL Libraries:

ANL-E

Main Library:

Lawrence Berkeley National Laboratory

Lawrence Livermore National Laboratory

Los Alamos National Laboratory

Naval Research Laboratory

Sandia National Laboratories

Energy Technology Division Review Committee:

M.L. Corradini, University of Wisconsin, Madison, WI

J.M. Deutch, Massachusetts Institute of Technology, Cambridge, MA

N.G. Eror, University of Pittsburgh, Pittsburgh, PA

C. Logan, Lawrence Livermore National Laboratory, Livermore, CA

M.A. Ulrickson, Sandia National Laboratories, Albuquerque, NM

R. Zoughi, University of Missouri-Rolla, Rolla, MO

J.C. Davis, retired from LLNL, 2262 Buena Vista Avenue, Livermore, CA

External:

M. Al-Rabban, Physics Department, Qatar University, Doha, Qatar

R. Anderson, Sandia National Laboratory, Albuquerque, NM

V. Bakshi, International SEMATECH, Austin, TX

D. Bolshukhin, XTREME technologies GmbH, Jena, Germany

R. Bristol, Intel Corporation, Santa Clara, CA

C. Bruineman, FOM Institute for Plasma Physics Rijnhuizen, Nieuwegein, The Netherlands

P. Choi, EPPRA SAS, Courtaboeuf, France

G. Derra, Philips GmbH, Forschungslaboratorien, Aachen, Germany

A. Egbert, Laser Zentrum Hannover, Hannover, Germany

A. Endo, Extreme Ultraviolet Lithography System Development Association, Kanagawa, Japan

S. Ellwi, PowerLase Limited, West Sussex, UK

B. Fay, Alcatel Vacuum Technology, Annecy, France

I. Fomenkov, Cymer, Inc., San Diego, CA

K. Gäbel, XTREME technologies GmbH, Jena, Germany

J. Gillaspy, National Institute of Standards and Technology, Gaithersburg, MD

S. Grantham, National Institute of Standards and Technology, Gaithersburg, MD

J. Greenwood, BOC Edwards, West Sussex, UK

Y. Izawa, Institute of Laser Engineering, Osaka University, Suita, Osaka, Japan

C-S. Koay, University of Central Florida, Orlando, FL

T. Kawamura, Institute for Laser Technology, Osaka, Japan

K. Koshelev, Institute of Spectroskopy, RAS, Troitsk, Russia

T. Kumazaki, Komatsu Ltd, Hiratsuka-shi, Kanagawa, Japan

R. Lebert, AIXUV GmbH, Aachen, Germany

E. Loius, FOM Institute for Plasma Physics Rijnhuizen, Nieuwegein, The Netherlands

K. Mann, Laser-Laboratorium Göttingen, Göttingen, Germany

P. Marczuk, Carl Zeiss Laser Optics GmbH, Oberkochen, Germany

M. McGeoch, PLEX LLC, Brookline, MA

H. Milchberg, University of Maryland, College Park, MD

T. Mochizuki, Himeji Institute of Technology, Kamigori, Akou, Hyogo, Japan

K. Nishihara, Institute of Laser Engineering, Osaka University, Suita, Osaka, Japan

T. Nishikawa, Faculty of Engineering, Okayama University, Okayama, Japan

J. Pankert, Philips Extreme UV GmbH, Aachen, Germany

J. Pomeroy, National Institute of Standards and Technology, Gaithersburg, MD

C. Rettig, Cymer, Inc., San Diego, CA

J. Ricardi, JMAR Technologies, Inc., San Diego, CA

B. Rice, Technology Development, Intel Corporation, Hillsboro, OR
M. Richardson, University of Central Florida, Orlando, FL
A. Sasaki, Advance Photon Research Center, JAERI-KANSAI, Kizu, Kyoto, Japan
M. Schuermann, JENOPTIK Mikrotechnik GmbH, Jena, Germany
F. Scholze, Physikalish-Technische Bundesanstalt, Berlin, Germany
L. Shmaenok, PhysTex, Nieuwegein, The Netherlands
U. Stamm, XTREME technology GmbH, Jena, Germany
K. Takenoshita, University of Central Florida, Orlando, FL
Y. Teramoto, EUVA, Gotenba, Shizuoka, Japan
Ch. Walton, Lawrence Livermore National Laboratory, Livermore, CA
Y. Watanabe, Canon Inc., Utsunomiya-city, Japan
O. Wood, International SEMATECH, Austin, TX
Ch. Ziener, XTREME technologies GmbH, Jena, Germany

Bibliothek, Max-Planck-Institute für Plasmaphysik, Germany
C.E.A. Library, Fontenay-aux-Roses, France
Librarian, Culham Laboratory, England
Thermonuclear Library, Japan Atomic Energy Research Institute, Japan
University of Wisconsin Library